N-1781
January 1988

NCEL
Technical Note

By T. A. Shugar, T. J. Holland,
and N. F. Shoemaker

Sponsored by National Science Foundation
Naval Support Force Antarctica

Collapse Prediction Analysis of South Pole Dome Due to Foundation Settlement

ABSTRACT The base of the geodesic dome sheltering the Amundsen-Scott South Pole Station is distorting due to movement in the compacted snow foundation. Determination of how much longer the dome can withstand ice field motion is aided by a nonlinear finite element analysis. A description of the base ring differential displacement is obtained by a least squares analysis of foundation displacement data. The topology and geometry of the geodesic dome have been reconstructed, and a one-to-one correspondence exists between the modeled and actual latticed framework. Two alternative approaches to structural modeling, based on the same topology, are developed and discussed.

Computational results are obtained, and then displayed and analyzed using computer graphics. These results indicate that the South Pole Dome can withstand twice the load currently induced by existing foundation settlement. The structure exhibits isolated group buckling but is in no danger of general collapse at that load level. The actual level of settlement at which general collapse could occur could not be calculated.

NAVAL CIVIL ENGINEERING LABORATORY PORT HUENEME, CALIFORNIA 93043

METRIC CONVERSION FACTORS

Approximate Conversions to Metric Measures

Symbol	When You Know	Multiply by	To Find	Symbol
		LENGTH		
in	inches	*2.5	centimeters	cm
ft	feet	30	centimeters	cm
yd	yards	0.9	meters	m
mi	miles	1.6	kilometers	km
		AREA		
in^2	square inches	6.5	square centimeters	cm^2
ft^2	square feet	0.09	square meters	m^2
yd^2	square yards	0.8	square meters	m^2
mi^2	square miles	2.6	square kilometers	km^2
	acres	0.4	hectares	ha
		MASS (weight)		
oz	ounces	28	grams	g
lb	pounds	0.45	kilograms	kg
	short tons (2,000 lb)	0.9	tonnes	t
		VOLUME		
tsp	teaspoons	5	milliliters	ml
Tbsp	tablespoons	15	milliliters	ml
fl oz	fluid ounces	30	milliliters	ml
c	cups	0.24	liters	l
pt	pints	0.47	liters	l
qt	quarts	0.95	liters	l
gal	gallons	3.8	liters	l
ft^3	cubic feet	0.03	cubic meters	m^3
yd^3	cubic yards	0.76	cubic meters	m^3
		TEMPERATURE (exact)		
°F	Fahrenheit temperature	5/9 (after subtracting 32)	Celsius temperature	°C

*1 In = 2.54 (exactly). For other exact conversions and more detailed tables, see NBS Misc. Publ. 286, Units of Weights and Measures, Price $2.25. SD Catalog No. C13.10:286.

Approximate Conversions from Metric Measures

Symbol	When You Know	Multiply by	To Find	Symbol
		LENGTH		
mm	millimeters	0.04	inches	in
cm	centimeters	0.4	inches	in
m	meters	3.3	feet	ft
m	meters	1.1	yards	yd
km	kilometers	0.6	miles	mi
		AREA		
cm^2	square centimeters	0.16	square inches	in^2
m^2	square meters	1.2	square yards	yd^2
km^2	square kilometers	0.4	square miles	mi^2
ha	hectares (10,000 m^2)	2.5	acres	
		MASS (weight)		
g	grams	0.035	ounces	oz
kg	kilograms	2.2	pounds	lb
t	tonnes (1,000 kg)	1.1	short tons	
		VOLUME		
ml	milliliters	0.03	fluid ounces	fl oz
l	liters	2.1	pints	pt
l	liters	1.06	quarts	qt
l	liters	0.26	gallons	gal
m^3	cubic meters	35	cubic feet	ft^3
m^3	cubic meters	1.3	cubic yards	yd^3
		TEMPERATURE (exact)		
°C	Celsius temperature	9/5 (then add 32)	Fahrenheit temperature	°F

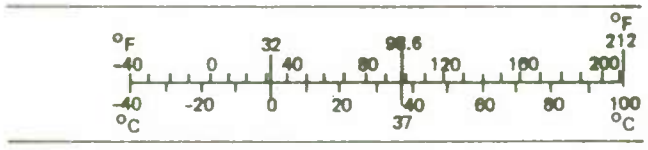

Unclassified

SECURITY CLASSIFICATION OF THIS PAGE (When Data Entered)

REPORT DOCUMENTATION PAGE		READ INSTRUCTIONS BEFORE COMPLETING FORM
1. REPORT NUMBER TN-1781	2. GOVT ACCESSION NO. DN666380	3. RECIPIENT'S CATALOG NUMBER
4. TITLE (and Subtitle) COLLAPSE PREDICTION ANALYSIS OF SOUTH POLE DOME DUE TO FOUNDATION SETTLEMENT		5. TYPE OF REPORT & PERIOD COVERED Final; Oct 1986 – Sep 1987 6. PERFORMING ORG. REPORT NUMBER
7. AUTHOR(s) T.A. Shugar, T.J. Holland, and N.F. Shoemaker		8. CONTRACT OR GRANT NUMBER(s)
9. PERFORMING ORGANIZATION NAME AND ADDRESS NAVAL CIVIL ENGINEERING LABORATORY Port Hueneme, California 93043-5003		10. PROGRAM ELEMENT, PROJECT, TASK AREA & WORK UNIT NUMBERS 64-094A
11. CONTROLLING OFFICE NAME AND ADDRESS National Science Foundation Naval Support Force Antarctica		12. REPORT DATE January 1988 13. NUMBER OF PAGES 63
14. MONITORING AGENCY NAME & ADDRESS(if different from Controlling Office)		15. SECURITY CLASS. (of this report) Unclassified 15a. DECLASSIFICATION/DOWNGRADING SCHEDULE

16. DISTRIBUTION STATEMENT (of this Report)

Approved for public release; distribution unlimited.

17. DISTRIBUTION STATEMENT (of the abstract entered in Block 20, if different from Report)

18. SUPPLEMENTARY NOTES

19. KEY WORDS (Continue on reverse side if necessary and identify by block number)

Structural analysis, latticed domes, finite element analysis, foundation settlement

20. ABSTRACT (Continue on reverse side if necessary and identify by block number)

The base of the geodesic dome sheltering the Amundsen-Scott South Pole Station is distorting due to movement in the compacted snow foundation. Determination of how much longer the dome can withstand ice field motion is aided by a nonlinear finite element analysis. A description of the base ring differential displacement is obtained by a least squares analysis of foundation displacement data. The topology and geometry of the geodesic dome have been

continued

DD FORM 1 JAN 73 1473 EDITION OF 1 NOV 65 IS OBSOLETE

Unclassified

SECURITY CLASSIFICATION OF THIS PAGE (When Data Entered)

20. Continued

reconstructed, and a one-to-one correspondence exists betwcen the modeled and actual latticed framework. Two alternative approaches to structural modeling, based on the same topology, are developed and discussed.

Computational results are obtained, and then displayed and analyzed using computer graphics. These results indicate that the South Pole Dome can withstand twice the load currently induced by existing foundation settlement. The structure exhibits isolated group buckling but is in no danger of general collapse at that load level. The actual level of settlement at which general collapse could occur could not be calculated.

Library Card

Naval Civil Engineering Laboratory
COLLAPSE PREDICTION ANALYSIS OF SOUTH POLE DOME DUE TO FOUNDATION SETTLEMENT (Final), by T.A. Shugar, T.J. Holland, and N.F. Shoemaker
TN-1781 63 pp illus January 1988 Unclassified

1. Structural analysis 2. Latticed domes I. 64-094A

The basc of the geodesic dome sheltering the Amundsen-Scott South Pole Station is distorting due to movement in the compacted snow foundation. Determination of how much longer the dome can withstand ice field motion is aided by a nonlinear finite element analysis. A description of the base ring differential displaccment is obtained by a least squares analysis of foundation displacement data. The topology and gcometry of the geodesic dome have been reconstructed, and a one-to-one correspondence exists between the modeled and actual latticed framework. Two alternative approaches to structural modeling, based on the same topology, are developed and discussed.

Computational results are obtained, and then displayed and analyzed using computer graphics. These results indicate that the South Pole Dome can withstand twice the load currently induced by existing foundation settlemcnt. The structure exhibits isolated group buckling but is in no danger of general collapse at that load level. The actual level of settlement at which general collapse could occur could not be calculated.

EXECUTIVE SUMMARY

The geodesic dome sheltering the Amundsen-Scott South Pole Station is settling into the compacted snow foundation. A structural analysis to determine the effects of the settlement, and to aid estimates of the life expectancy for the structure has been conducted. The analysis strategy is to simulate the settlement process incrementally until a collapse condition for the structure is determined.

The South Pole Dome is considered a single layer latticed dome. Collapse analysis and particularly post-collapse analysis of such structures remains very much a research issue, and is an ad hoc procedure in the practice of structural analysis. In this investigation, both linear and nonlinear three-dimensional finite element technology has been applied to the solution. Commercially available software running on a Cray super computer was employed, and computer graphics were used to analyze response data.

A mathematical procedure was developed to analyze field data of the structure's settlement which was based on the method of least squares. This procedure determined the rigid body settlement and the differential settlement components of the field data. The latter component is of interest to structural analysis. The maximum differential settlement calculated is 5 inches. The maximum rigid body rotation calculated is 0.67 degrees. Rigid body settlement in the vertical direction could not be determined for lack of a reference elevation.

For the sake of completeness, conventional loads of gravity, snow, and wind were also considered in this study. The snow load was calculated from field data on the depth of the snow-berm accumulation on the leeward side of the dome. In effect, this analysis resulted in a snow-berm load condition. The snow berm extends some distance downwind from the dome. The best physical explanation of the cause of the settlement sustained by the dome is that the weight of the snow berm is compressing the field of precompacted snow beneath the berm.

The full three-dimensional geometry and topology of the South Pole Dome framework structural model was reconstructed in the absence of design drawing information. The framework topology includes a one-to-one correlation between the joints and member length for the structural model and the actual dome. The coordinates of the joints agree with known overall geometry and the lengths of the various members agree with the available field measurement data and are consistent with overall geometry. There are 565 joints and 1,550 members in the framework topology including the base ring. Additionally, 915 triangular plate bending members were used to simulate the behavior of the dome's cladding. Overall, the structural model of the South Pole Dome possess nearly 3,400 degrees of freedom. That is, nearly 3,400 displacements are computed over the surface of the Dome for each load case studied.

Linear structural analysis studies of the South Pole Dome were aimed at analyzing the condition of the structure in its present state. Computed member bending stresses for all load cases are below 1,000 psi and are therefore negligible. The computed structural response of the South Pole Dome due to foundation settlement is greater than the effect of the snow-berm or wind load cases. The response of the structure considering the settlement load case alone is, however, well confined to

framework members located down low in the dome near the base ring where the settlement displacements are imposed. Member stresses for this load case are less that 12,500 psi.

When the foundation settlement load case is combined with the snow-berm and wind load cases, the maximum member stresses are computed to be about 50 percent less than yield, which is 36,000 psi for aluminum alloy. These results tend to confirm the structural integrity of the South Pole Dome in its present condition.

In the nonlinear analysis, settlement displacements were successfully simulated incrementally up to a level of twice the existing settlement level. Behavior of the framework at this level of settlement remained linear. The highest stressed member possessed an axial stress of 25,800 psi. Thus, all members were stressed below yield. It was also determined that members would not buckle in the elastic range.

Just beyond twice the existing level of settlement load, the nonlinear analysis results did indicate that group buckling occurred at isolated locations on the leeward surface of the dome. In this mode of buckling, a joint, into which several members frame, suddenly displaces a small amount in a direction normal to the dome's surface. Bending stress suddenly appeared in the connecting members. However, there was no evidence in these results of formation of a general state of structural collapse of the dome.

It was concluded that the South Pole Dome could sustain at least twice the existing level of foundation settlement without being in danger of reaching a general state of structural collapse. However, the level of foundation settlement that would correspond to a general collapse condition for the South Pole Dome could not be calculated.

CONTENTS

INTRODUCTION

Metal, shell-like latticed structures are very popular. They are low in cost and weight, and often they can be prefabricated and erected at remote sites. However, procedures for structural analysis of shell-like lattice structures remain ad hoc, for they cannot easily exploit the classical analysis methods developed for continuous isotropic shells in the sense of Timoshenko and Woinowsky-Krieger (1959).

Investigation of the collapse behavior potential of a single-layer latticed dome due to base ring distortion is a particularly unusual task. Very little information exists in the literature on the subject, as compared with collapse analysis methods involving direct loading. See, for example, the bibliography compiled by the ASCE Task Committee on Latticed Structures (1976).

The foundation of the geodesic dome at the Amundsen-Scott South Pole Station is settling with movement in the compacted snow foundation. An estimate of the life expectancy of the dome is aided via a nonlinear finite element structural analysis. The goal of the analysis is to predict the relationship between progressive collapse of the structure and advancing stages of foundation distortion. The structural analysis calculations were made using a commercially available general purpose nonlinear finite element program running on a Cray computer. The loading consists of prescribed incremental displacements, and the analysis is fully three-dimensional and includes the effects of large displacements in member response. The material model used was linear elastic. The effects of simultaneously acting wind and snow loads are included. A preliminary structural analysis of the South Pole Dome was conducted by Shugar et al. (1987) and Shugar and Holland (1987).

The South Pole Dome was designed to be a weather break that shelters the scientific station communications center, crew quarters, and laboratories from wind and snow. Construction materials for the dome were airshipped to the Pole in 1972, and since its construction in Deep Freeze 73 (DF 73 is July 73 to June 74) it has sustained substantial foundation settlement according to recent onsite surveys. This is a historical problem for structures at the South Pole site (ENR 1969 and Curtiss 1983).

The 1987 NCEL site survey data (Lunsford, 1987) is carefully analyzed to obtain a picture of base ring settlement. Differential settlement is of primary concern. This component is separated from the rigid body component of the total base ring settlement to provide the basic structural loading to which the dome is subjected.

Regarding the structural model, discussion is given as to the idealization of the lattice members as either nonbending (truss) members or bending (frame) members. The latter idealization was employed in the model. The cladding is modeled to interact with the latticed framework, and is idealized as a (faceted) fully bending thin shell.

Static linear and nonlinear analyses were employed. In the nonlinear analysis the strategy was to apply idealized differential displacements incrementally to the base ring in magnitudes sufficient to lead up to collapse of the dome.

The structural analysis results are presented using computer graphics. Member stresses and structure deformations at various stages of loading are shown and analyzed.

GEODESIC DOME CONFIGURATION

The South Pole Dome is shown in Figure 1. The structure is regarded as a single-layer latticed dome, and as shown in Figure 2, is 164 feet in diameter and 53 feet high at the crown. It is composed of three primary substructures: a latticed framework, an outer cladding, and a tension or base ring. The dome is constructed entirely of aluminum alloy. The dome's spherical shell is composed of five topologically identical 72-degree sectors. The individual members of the latticed framework in each sector are made in 12 different lengths which vary from 8 feet to 10 feet. They are exclusively 6-inch-deep WF-sections. Gusset plates are used to join the members at the nodes.

Triangular plates, 0.050 inch thick, constitute the outer surface cladding of the dome. The plates are attached to the framework at their three vertices and along their three edges. The primary method of attachment is by bolting at the three vertices. Along the edges, a mechanical or articulated seal is employed instead of a continuous structural joint. A hole in the cladding at the apex of the dome serves to bleed off heat.

The base ring is functionally a tension ring. The inner and outer chord (outrigger chord) members of the tension ring are lag-bolted to 70 evenly spaced timber pads.

FOUNDATION DISPLACEMENT

The measured displacement of the base ring includes two types of displacement: rigid body translation and rotation, and differential settlement (Shugar, et al. 1987). The latter information is critical to the structural analysis of the dome. The former is of value in understanding the onsite, gross motion of the dome. Because of the unique behavior of the compacted snow material in which the South Pole Dome is founded, the dome may not only be settling, but it also may be distorting in the plane of the dome's floor.

To determine the magnitudes of the rigid body translation and rotation, a least squares procedure was used to fit a plane through the measured vertical displacement data of the base ring. This procedure is illustrated in Figure 3.

The equation of the plane containing the rigid body position of the base ring is:

$$z = \bar{z} + \theta_y x + \theta_x y$$

where the coefficients define the magnitudes of the rigid body displacement as follows:

$\bar{z}$ = vertical translation from the "original" floor position

θ_y = rotation about a horizontal y axis

θ_x = rotation about a horizontal x axis

The data used for the least squares analysis were taken from the site survey conducted by the Naval Civil Engineering Laboratory (NCEL) in January 1987 (refer to Lunsford (1987) for further details).

The least squares analysis identifies the coefficients in the equation of the plane. They are presented in Table 1.

Table 1. Computed Rigid Body Settlement of the South Pole Dome

Translation ($\bar{z}$)*	=	0.5 feet (upwards) from surveyors arbitrary origin
y-axis rotation (θ_y)	=	-6.145×10^{-3} radians (cw)
x-axis rotation (θ_x)	=	1.069×10^{-2} radians (ccw)

*The translation component is not meaningful for there was no correct datum elevation established for referencing vertical translation.

A snow berm has accumulated on the leeward side of the dome and it continues downwind some distance (see Figure 1). The weight of this berm is apparently consolidating the otherwise free field beneath the berm. This was first discussed by Curtiss (1983). This consolidation would only roughly explain the direction of the computed rigid body rotation. Cracks have formed on the compacted snow floor inside the dome and seem to be involved in how the dome rotates. The mechanical properties of the compacted snow field are also probably anisotropic. The existence of a tunnel, called the Utilidor, beneath the compacted snow floor is also a factor in the crack pattern in the floor. These four factors all have an influence on how the dome moves, and complicate any simple explanation of its motion.

The differential settlement of the base ring is obtained by subtracting the computed rigid body settlement of the base ring from the total settlement. It is shown graphed about the circumference in Figure 4. The maximum differential settlement is 5 inches.

The differential displacement data can be directly input to the finite element analysis computer program in preparation for a structural analysis of the South Pole Dome. Alternatively, the total displacement data can be prescribed as input data. The same structural response should be achievable by either method. In the present analysis, the differential displacement data were used as input data.

The differential displacement data were smoothed to minimize numerical difficulty before they were prescribed. The irregularity in the data stems naturally from the measured data. Finite element analysis software has computational difficulty with large amounts of prescribed displacement data that vary irregularly. This creates many highly concentrated effects which result in equilibrium difficulty in the complete structure. The irregularity in the data is due to measurement errors and construction errors (imperfections). Since the gross behavior of the dome due to settlement is of interest, the data were smoothed to filter out local irregularity.

For purposes of numerically predicting collapse, it is the basic shape of the differential displacement data, as contrasted with absolute magnitude, that is important. Therefore, the input data are normalized as well as smoothed. The applied displacements are prescribed incrementally in steps, a method analogous to proportional loading with direct forces or pressures. The strategy of applied incremental displacements would then be to continue their application until the magnitude of the displacements that correspond to a general collapse condition of the dome is determined.

These data could then be compared to the historical rate of displacement, as determined by an auxiliary analysis of the annual site survey data, to predict the structural life span expectancy of the South Pole Dome. This strategy obviously assumes that the shape of the displacements remains constant with time. The magnitude of the displacements may be assumed to vary linearly or nonlinearly with time depending on historical data on the rate of settlement. Analysis of such data conducted elsewhere (Lunsford, 1987) indicated that displacement magnitudes tend to increase linearly.

GRAVITY, SNOW, AND WIND LOADS

To obtain a complete structural analysis, conventional loads were also considered in this study. Linear shell membrane solutions are available for continuous domes for gravity and wind load conditions. If the South Pole Dome is idealized as a continuous shell, these solutions, from the membrane theory of shells, provide useful and economical insight into the structural behavior of the dome, and useful background for any proposed nonlinear analysis of shells. These solutions are provided in Appendix A.

The conventional loads of gravity, snow, and wind acting on the South Pole Dome are depicted in Figure 5. The basic load data for each condition are discussed in the following.*

The corresponding uniform gravity load condition is depicted in Figure 5(a). The spherical radius r of the dome is 90.2 feet. The structural analysis computer program computes the gravity load independently; however, the value of p_g is estimated to be 3 lb/ft^2.

*Thermal loading in this study was disregarded. The South Pole Dome was designed to minimize the temperature difference between inside and outside the dome.

Site survey data of the snow-berm accumulation on the leeward side of the dome enables the depth of the accumulation at stations around the perimeter to be quantified. An idealization of the snow load condition is depicted in Figure 5(b).

The pressure of the snow berm is assumed to be active and hydrostatic; that is, pressure acts in a direction normal to the dome surface and has a linear distribution with depth. The usual assumption is that snow load acts vertically. However, the snow material at the South Pole is unusually constituted of a granular structure, and would tend to behave actively rather than passively while bearing on the dome. Thus, the hydrostatic assumption is justified.

Hydrostatic pressure of the snow load is described by the equation:

$$p_s = (1-ky)\ \gamma_{snow}$$

where γ_{snow} is the unit weight of the snow-berm material. The mass density of the material has been measured by NCEL personnel, and is 0.314 g/cm^3, which represents a unit weight of 19.7 lb/ft^3. The geometrical quantities 1, m, and k define the region of the dome over which the pressure acts. Their values calculated from the site survey data, are, respectively, 37.6 feet, 52.8 feet, and -0.209.

This load condition is regarded as permanent, and is treated as a dead load. Consequently, like the load of the structure's weight, the snow load is assumed to act simultaneously with the loads from wind and foundation settlement. This is a departure from conventional structural analysis of expeditionary structures where wind and snow load conditions are ordinarily analyzed independently because they are not likely to occur simultaneously. However, it is prudent to consider the snow berm permanent at the South Pole Dome site.

The wind load condition arises from the transfer of kinetic energy from the free stream wind velocity to strain (potential) energy of deformation of the dome shell surface. The free stream wind (or dynamic) pressure is given by the equation:

$$p_o = 0.00256\ V^2$$

where V is the wind velocity in mph and p_o has units of psf. A 200-km/h wind velocity was used in the present analysis in the absence of specific data on local weather conditions. The corresponding static pressure normal to the dome surface is the product of the free stream pressure and a locally varying static pressure coefficient. This is given by the equation:

$$p_w = p_o \sin\phi \cos\theta$$

The wind load parameters are depicted in Figure 5(c).

As can be seen from the above equation, the pressure is positive (inward) on the windward side of the dome, and negative (outward) on the leeward side of the dome. On the portion of the leeward side where the snow berm exists, the wind pressure is regarded as zero. The aerodynamic effect of the snow berm is unknown and is otherwise disregarded in this analysis.

STRUCTURAL ANALYSIS MODEL

A fully three-dimensional finite element analysis model is necessary to accommodate unsymmetrical load conditions and anisotropic structural conditions of a latticed framework. Obtaining a solution for a shell problem is ordinarily dependent on the geometry, loading, and boundary conditions. Continuous geometry, smooth loading, and idealized boundary conditions are generally required to obtain analytical solutions. Where deviations from any of the preceding complicate the analysis, an analytical solution may not be possible and under these conditions the analyst may resort to numerical techniques, the most prominent of which is the finite element method.*

Since the finite element method is a bona fide three-dimensional structural analysis method that handles discrete systems such as latticed frameworks, it is a sound basis for collapse analysis of domes that conveniently and systematically takes into account their structural anisotropy.

A significant analytical effort was required to reconstruct the topology and geometry of the South Pole Dome due to the unavailability of detailed design drawing information. An erection manual for the dome that contained only overall dome dimensions and code numbers used for assembling variable-length members into the lattice work was the only design information available. This was supplemented by actual field measurements of member lengths made by NCEL personnel. Combining this information, a mathematical procedure was developed and programmed for the computer to determine the topology and geometry of the entire dome. The principal output data of this program are the x, y, and z coordinates at each joint in the dome. The results of the reconstructed South Pole Dome topology and geometry are illustrated graphically in Figure 6. The reconstructed topology and geometry as shown is an accurate replication of the topology and geometry of the South Pole Dome, member-for-member and joint-for-joint. Apperatures in the dome for entry and exit are disregarded. However, the pentagonal hole at the apex is included in the model.

Two different structural models of the South Pole Dome framework employing the same topology and geometry were considered: a truss model and a bending model. Which formulation to use appears to be an unresolved issue in the research community. In practice, the choice is often restricted to the elements available for nonlinear analysis in the software that is being employed. This issue is reflected in Figure 7, and is discussed below.

---

*As an alternative to the finite element method of analysis, it is possible to conceive of analytical approaches which would rely more on classical shell bending and buckling theory. Mullord (1984) discusses two such alternatives to numerical approaches. One is based on elastic stability, and the other is based on plasticity and is akin to yield line theory for flat plates. Such approaches require that an equivalent continuous shell structural model be devised by a procedure that smoothes or averages the obvious anisotropy in a latticed dome.

In the analysis of planar truss structures it is generally assumed that the individual struts are connected by ideal articulations, i.e., without bending resistance. Hence the struts are not subjected to moments or shearing forces, but to axial forces only. This assumption simplifies the calculation considerably since disregarding moments often leads to a statically determinate system. The hypothesis of ideal articulations is, however, not generally in accordance with the actual construction of the truss structure. The top and bottom chords of the trusses are normally continuous through several panel points. Thus, the flexural resistance of such points is not only not equal to zero but, because of gusset plates, is larger than anywhere else.

The applicability of the truss theory derives from another fact: if we calculate a truss with rigid connections as a highly statically indeterminate system by using the corresponding idealized truss as a substitute system on which we apply the moments as unknowns, then we obtain for these unknowns values of such small magnitude that we can neglect them completely. Thus, as far as the final result of the calculations is concerned, bending stresses are of secondary importance in linear truss structures.

Thus, a finite element truss model of the dome assumes an ideally articulated, momentless joint in spite of the gusset plates into which each member frames, and the members develop only axial force in spite of their bending and torsional rigidity. Such a model also assumes the loading on the dome has only a small component normal to the dome surface. A primary consequence of these assumptions is that the order of the finite element truss model is dramatically decreased. This is particularly advantageous in a nonlinear structural analysis setting, but the nonlinearities and the normal load component must remain small for the truss model to be accurate.

The type of finite element that may be specified for the dome members in a truss model is a two-node, linear-displacement truss element with 3 degrees of freedom at each node. It may be used in the context of a large displacement, updated Lagrangian formulation to capture nonlinear behavior.

While it is believed that a truss model could strike a balance between accuracy and computational cost, there is no question that a bending model of the South Pole Dome's framework would be more accurate, particularly for nonlinear analyses. Such a model could also potentially provide a more robust procedure by minimizing premature buckling at the joints and numerical instability during analysis.

During group buckling a group of members framing into any one node moves dramatically in a lateral direction. The resistance to this mode of buckling would depend on the end fixity condition of the members. In the bending model of the dome, full fixity is assumed in the absence of experimental data to the contrary. The truss model, by comparison, would assume zero fixity and is a more conservative model relative to group buckling albeit more susceptible to premature numerical instability.

The question of whether to use a truss model or a bending model to replicate the South Pole Dome framework's load-deflection behavior was studied further and is addressed in Appendix B. Using models of a representative substructure of the dome's framework, it was determined that a bending model is more suitable. The primary loading to which the

dome is subjected, foundation settlement, may be expected to cause bending moments in planes normal to the dome's surface, and therefore require the normal stiffness of the framework to be modeled correctly. Only the bending model can accomplish this as demonstrated in this study. No satisfactory results were obtained from the nonlinear truss model. Numerical instability resulted for load steps as small as $0.025\ \bar{\delta}$, and this behavior is inconsistent with the observed structural condition of the dome in the field.

A two-node one-dimensional frame element with 6 degrees of freedom at each node could be used in the bending model of the South Pole Dome framework. This element precludes the possibility of local buckling behavior of any strut in the dome unless it also possesses special experimentally-based constitutive relations. However, the possibility of group buckling behavior is retained. Local buckling could be considered by subdividing each strut in the framework into two or more of these elements, albeit at much greater cost. However, in this case, a geometrically nonlinear implementation of this element was not available and it could not be considered.

Solid, isoparametric two-node elements would seem to offer computational advantages over alternative two-node, solid frame elements such as a Hermitian element. Both these elements may be used with nonlinear analyses in ADINA. To avoid shear locking and retain accuracy, the isoparametric formulation requires that the element stiffness matrix be evaluated by reduced numerical integration (see Bathe 1982). Therefore, we could specify only one-point Gaussian quadrature in the direction of the element and thereby achieve added efficiency. In the transverse directions we would be constrained to using four-point quadrature.

However, an auxiliary analysis using coarse models of the dome framework showed that the Hermitian element was more accurate and satisfatory for our purpose than two- and three-node isoparametric elements. Thus, the Hermitian solid element formulation was used to model the South Pole Dome framework.

Solid frame elements cannot replicate all the actual section properties of a frame member. In that event we chose to assign the properties of the frame element's equivalent rectangular cross-section dimensions that correspond to the actual member area, and the actual member major axis inertia. Actual and equivalent sections are sketched in Figure 8 for the South Pole Dome. The minor axis inertia and the torsional constant are thereby constrained to be very different from their actual values, as shown in Table 2.

Concern arises for accurate behavior of solid frame elements assigned equivalent section properties. Do the differences between actual and equivalent section properties matter in the case of the present study? This question was investigated and further reported on in Appendix C. The investigation concluded that the solid frame element with the equivalent section properties shown in Table 2 models the stiffness of the South Pole Dome framework in both the tangential and normal directions adequately.

Table 2. Actual and Equivalent Section Properties for South Pole Dome Frame Members

	Actual Section Properties	"Equivalent" Solid Section Properties	Error
Frame Member:			
Area, A	3.66 $in.^2$	3.63 $in.^2$	0.7%
Strong Axis Inertia, I_{xx}	25.11 $in.^4$	24.95 $in.^4$	0.6%
Weak Axis Inertia, I_{yy}	5.86 $in.^4$	0.04 $in.^4$	large
Torsion Constant, J	25.78 $in.^4$	0.194 $in.^4$	large
Base Ring:			
Area, A	--	7.11 $in.^2$	--
Strong Axis Inertia, I_{yy}	--	2,077 $in.^4$	--
Weak Axis Inertia, I_{xx}	--	0.11 $in.^4$	--

The cladding structure is also included in the finite element model.* The triangular plates that constitute the dome's cladding could be modeled as plane stress elements, where once again, bending is neglected. The bending rigidity of the plate is thereby regarded as negligible compared to its inplane or stretching rigidity. The dome's cladding taken as a whole, exclusive of the framework, would therefore behave as a faceted shell membrane, i.e., with the intentional neglect of normal shear, bending moment, and twisting moment.

A linear-displacement, quadrilateral finite element could be specified to model the triangular cladding plates. In this procedure, two adjacent nodes are coalesced to form a triangular element. This is a common procedure when existing, standard, three-node plane stress elements are otherwise not available, but there is a concern for accuracy under general circumstances with this procedure.

The plane stress element and the truss element described above linearly interpolate the displacement field within each element. Thus, full displacement compatibility is thereby imposed between the struts and edges of the plates in the structural model. In this way, the cladding and the lattice framework are assumed to fully interact in resisting load. However, this may not be desirable. Recall that this joint is not continuous in the actual structure.

*In experimental work on a parabolic cylindrical roof structure constructed of cladding and arch ribs, Zhao, et al. (1984) found the cladding can carry as much as 60 percent of the force carried by the arch ribs. This would indicate the cladding should not be ignored in the structural model of the dome.

In a bending model, the cladding could be simulated by plate bending elements. These elements possess 6 degrees of freedom per node. When assembled with the beam elements in the structural model they do not increase the number of global degrees of freedom. Additional computation is required for the plate element matrices over and above that required for plane stress elements in a nonbending formulation. Here again, reduced numerical integration may be prescribed which partially offsets their increased computational cost.

Two different plate bending elements were investigated as to their stiffness behavior for use with the South Pole Dome model. This investigation is summarized in Appendix D. The discrete Kirchoff plate element (see Bathe, 1982) performed well based upon an evaluation of overall combined stiffness of frame elements and plate bending elements. This element was used to model the effect of cladding in the South Pole Dome model. It contributes 24 percent to the total stiffness of the dome in the normal direction.

Size characteristics of the alternative South Pole Dome finite element models are given in Table 3. These are regarded as moderate sized models in the context of nonlinear problems depending on the computational power of the computer employed.

Table 3. Alternative South Pole Dome Models

	Truss Model	Bending Model
No. of Truss Elements	1340	0
No. of Plane Stress Elements	915	0
No. of Plate Elements	0	915
No. of Beam Elements	210	1550
No. of Node Points	565	565
No. of Degrees of Freedom	1691	2833
Half Band Width	612	677

LINEAR STRUCTURAL ANALYSIS RESULTS

The purpose of the linear structural analysis conducted in this investigation is two fold: (1) to serve as a precursor to the nonlinear analysis, and (2) to evaluate the structural condition of the South Pole Dome relative to the present state of foundation settlement and conventional load conditions of snow and wind. The ADINA (1984) finite element program was used in this analysis.

As it turned out, the member bending stresses computed in the linear analysis were less than 1,000 psi everywhere for all load conditions and are therefore neglected. In the following discussion, only member axial stresses computed from the linear analysis are reported.

Results are shown by using computer graphics that highlight only those members sustaining stress greater than 1,000 psi absolute within the dome framework. Tension and compression stresses are distinguished in these graphics. The dome framework is oriented relative to the direction of prevailing weather at the South Pole site for reference. Both plan and elevation views are shown. In the latter, the view is in the direction of the wind, looking slightly up and under the framework.

The computed member stresses for the snow-berm load case are shown in Figure 9. It is clear that this load case is not significant by itself, for the maximum member stress throughout the framework is only 1,460 psi compression. As expected, the response is localized to the lower members beneath the snow berm and symmetrical about a diametrical plane in the direction of the prevailing weather.

The above results were obtained with the displacements of the base ring completely fixed. Thus, the computed stresses in the base ring members are constrained to be zero. However, for the snow-berm load condition, it might be just as reasonable to assume that base ring displacements in the horizontal plane should not be fixed. This would be consistent, for example, with a passive material model for the surrounding compacted snow foundation. The member stress response for this condition was also obtained, though it is not shown here. The stresses in the dome framework remain about the same, i.e., very small. The maximum member stress in the structure is a tension stress which occurs in the base ring for the snow-berm load condition when the base ring is free to displace in the horizontal plane.

The computed response of the South Pole Dome due to a 200-km/h wind load is shown in Figure 10. An interesting pattern of member stress occurs with compression and tension occurring in the windward and leeward members, respectively. This classic overall behavior is typical of wind loading on spherical domes of uniform thickness and isotropic construction. However, the detailed member response shown is not typical and is due to the particular anisotropic construction of this latticed dome.

The maximum stress is 2,090 psi tension on the leeward side. The maximum compression stress is 1,680 psi on the windward side. In either case, it appears that the stress is remarkably small for a 200-km/h wind velocity. These stress levels are as insignificant as those that occurred for the previous, snow-berm load case. The difference is that wind load produces a uniform stress distribution while the snow-berm load produces a localized stress distribution. As mentioned, the member bending stresses are negligible even though displacements of the base ring were constrained to be zero for this load condition.

A variation on the wind load case was studied where the load on the leeward side was excluded from the surface covered by the snow berm. The results for this partial wind load case are shown in Figure 11. The maximum stresses are slightly reduced for this case, and fewer members are stressed beyond 1,000 psi. The snow berm therefore does provide a wind break on the leeward side, but the level of member stress in either case is very low. The partial wind load case is also used in a combined load case study which is discussed later.

The response of the structure to the settlement loads is shown in Figure 12. The vertical displacements imposed on the base ring are equal in magnitude and distribution to the existing differential settlement as calculated in this study from analysis of the 1987 NCEL site survey data. The base ring displacements in the horizontal plane are assumed to be unconstrained in these data, and develop as a response to the imposed vertical displacements. These can be seen in the distorted shape of the base ring in Figure 12(b). In this figure the displacements are magnified for visibility and are not to scale.

It is clear from these displacement results that an imposed differential settlement will also cause out-of-roundness in the base ring if displacements in the horizontal direction are not constrained by the foundation (see Figure 12a). In this analysis, we assume that they are not constrained. This would be more consistent with a viscoelastic or passive model of the compacted snow foundation's material behavior. That is, if subjected to a load, the material will give way gradually over time (creep) until the load either diminishes or vanishes altogether.

The maximum member stress due to the settlement load is 12,600 psi compression. This is about six times greater than the maximum stress obtained from either the wind or snow-berm load case. Thus, the settlement load condition is much more significant than the conventional load conditions. The stresses are confined to members located near the base ring, and correspond to areas of greater differential settlement; in this case mostly to members near the leeward edge of the dome.

The response of the South Pole Dome to combined gravity, snow-berm, 200-km/h wind, and existing settlement loads is shown in Figure 13. Computed displacements and member stresses are both included in the figure.

Displacements in the horizontal plane are unconstrained, consistent with the more important load case of settlement. Thus, the effects of snow-berm and wind loading as discussed above are not exactly superimposed here, for they were associated with the boundary condition of fixed or constrained base ring displacements in the horizontal plane.

The maximum member tension stress is 11,400 psi and the maximum member compression stress is 13,200 psi for the combined load case. These stresses are consistent with a simple superposition of the stresses from the individual load cases. They are well below the 36,000 psi yield stress for aluminum alloy. Thus, considering very general load conditions, the South Pole Dome's existing structural integrity is established according to the results of the present linear structural analysis.

NONLINEAR STRUCTURAL ANALYSIS RESULTS

The ADINA (1984) general purpose nonlinear finite element computer program was also employed in this nonlinear analysis of settlement loads. Further, solution option A was selected to predict post-collapse behavior. An overview of computational aspects of post-collapse behavior is given in Appendix E. It was not possible with this program to consider nonlinear analysis of the combined load condition for the dome.

The prescribed settlement load for the nonlinear analysis consisted of deforming the base ring to twice the value of the existing deformation as obtained from the 1987 NCEL site survey data, which is denoted

here as 1.0 $\bar{\delta}$. Results for the load levels of 0.647 $\bar{\delta}$, 1.095 $\bar{\delta}$, 1.544 $\bar{\delta}$, and 1.992 $\bar{\delta}$, are presented graphically for the bending model in Figure 14. In this figure the deformed shape (enhanced for visibility) of the dome base ring can be seen to gradually increase. The axial stresses in the members of the dome in units of psi are indicated for members sustaining stress greater than 2,500 psi absolute.

The results reported here were obtained from the bending model of the dome. The base ring is assumed to be restrained against rotation. This boundary condition, although not completely correct, better models the torsional resistance of the tension ring (see Figure 2(b)), which is believed to be high because it is lag-bolted to timber pads that are embedded in the compacted snow foundation.

The bending model results show the large majority of the dome's members are unaffected by settlement of the foundation. Only members located near the base ring are affected. The response is well confined to the region of differential settlement.

The member response exhibits essentially a linear behavior up to 2.0 $\bar{\delta}$. Thus, according to these bending model results, nonlinear kinematic effects are also expected to be slight even when the existing foundation settlement has doubled.

The calculated mean member force is noted to be consistently near zero. There are two reasons for this. First, the majority of the members contain very small forces. Second, a count of the compressed and stretched members shows that their numbers are nearly equal, so that there is a cancelling effect when calculating the mean force. This latter observation is apparently typical structural behavior of systems possessing topologies that are based on the triangle, whether they are simple planar trusses, or complex, three-dimensional geodesic domes.

Considering the maximum stress in the members for load level 2.0 $\bar{\delta}$, the ratio of the yield stress to the maximum axial stress is nowhere in the dome framework less than 1.40. Further, assuming strong axis buckling, the Euler buckling stress for a typical member exceeds the yield stress so the members will not buckle elastically. Since member stresses are less than yield, member buckling is precluded. This also verifies the choice made in modeling the members which implies members would not buckle.

Just beyond load level δ = 2.0 $\bar{\delta}$, evidence of group buckling in the numerical computation occurs. At load level δ = 2.19 $\bar{\delta}$, significant bending stress suddenly appears in a few isolated members. To this point in the loading, bending stresses have been negligible. For example, the maximum bending stress anywhere in the framework at δ = 2.0 $\bar{\delta}$ was ±124 psi. Now, due to a mere 10 percent increase in load level, the maximum bending stress is ±14,400 psi. Members sustaining bending stress and axial stress greater than 2,500 psi absolute are shown in Figures 15 and 16, respectively, for load level δ = 2.19 $\bar{\delta}$. At this load level, combined stresses for certain members could exceed the yield stress, but they would be isolated members if indeed they exist at all. Thus, the structure may be said to be locally unstable at this settlement load level. The results do not indicate widespread group buckling or general instability for the dome. It would be advisable, however, to monitor future, normal displacements in the dome's framework in locations such as those shown in Figure 15.

Beyond this point in the numerical simulation, program execution failed. The program was unable to assemble a stable structure stiffness matrix. It reported 26 negative eigenvalues had been detected for this matrix. It was believed that computation of further post-buckling configurations should have been achievable with continued application of the load using solution option A. Several attempts to adjust the computational parameters were made in an effort to restart the computation but to no avail. The particular formulation implemented in the software used for surmounting computational difficulty at the point of buckling was not sufficiently robust in this instance.

Thus, it was not possible to calculate the settlement load level at which general collapse of the South Pole Dome would occur. However, the results do indicate that the South Pole Dome could withstand twice the existing level of foundation settlement that it presently sustains. This finding is made in the absence of consideration for the combined load effects from snow and wind. However, the linear analysis showed that these effects were small.

SUMMARY AND CONCLUSIONS

A structural analysis of the geodesic dome sheltering the Amundsen-Scott South Pole Station was conducted. The analysis emphasized structural collapse due to foundation settlement. Three-dimensional structural models of the South Pole Dome were prepared and analyzed based on the application of commercially available nonlinear finite element technology. The finite element model topology and geometry for the South Pole Dome were carefully reconstructed. There is a one-to-one correspondence between the struts, panels, and joints of the dome and the struts, panels, and joints of the finite element model.

An auxiliary method for analyzing the data from the 1987 NCEL site survey of foundation settlement was developed based on the mathematical method of least squares. It yielded a detailed picture of the dome's rigid body rotational displacement and the distortion in the base ring. The latter component provided the necessary data for simulating the prescribed displacement loading to which the base ring of the dome is subjected in the structural analysis.

Direct specification of measured base ring settlement data could not be accommodated computationally by the nonlinear structural analysis software used. The measured data is too irregular. The solution was to smooth the data and prescribe an idealized version of the differential settlement data instead. This helped to minimize the number of ineffective computer runs, and provided more reasonable computed response while also simulating the primary differential displacement pattern inherent in the measured data.

A linear structural analysis was conducted to assess the South Pole Dome's structural integrity relative to the present state of foundation settlement. This analysis also included the conventional loads due to gravity, snow, and wind. It was found that response of the dome due to settlement alone is more onerous than due to the conventional loads. However, the response due to even the combined load condition shows that framework members are stressed well below yield. The South Pole Dome, in its present state, is structurally adequate according to results from the linear analysis.

Results from the bending model of the nonlinear finite element analysis showed that the dome could sustain at least twice its existing differential settlement without significant structural consequences. At this level of settlement, no group buckling in the dome's latticed framework was in evidence. Further, the structure behaved linearly at this level of loading and maximum axial stresses in the framework were less than yield. Member bending stresses were negligible throughout the framework. However, after incrementing the load just beyond twice the existing settlement, evidence of group buckling occurred in two widely separated locations on the leeward side of the South Pole Dome. Bending stresses for members at these two locations increased dramatically. There is a possibility that combined axial and bending stresses could exceed yield in these members but their number remains small and they are isolated locations. There is no evidence of widespread occurrences of group buckling that would indicate a general state of structural collapse for the South Pole Dome at this level of settlement loading.

The computer analysis was unable to follow the load-deflection behavior of the South Pole Dome beyond an initial, localized post-buckling configuration. Therefore, the settlement level at which general collapse of the dome would occur could not be predicted.

ACKNOWLEDGMENTS

Support for this investigation was provided by the Naval Support Force Antarctica and the Division of Polar Programs of the National Science Foundation.

REFERENCES

ADINA Engineering, Inc. (1984). ADINA Users Manual, Report AE 84-1-2. 71 Elton Ave., Watertown, MA 02172, Dec 1984.

Bathe, K.J. (1982). Finite element procedures in engineering analysis. Englewood Cliffs, N.J., Prentice-Hall, Inc., 1982.

Bathe, K.J., and Dvorkin, E.N. (1983). "On the automatic solution of nonlinear finite element equations," Computers and Structures, vol 17, no. 5-6, 1983, pp 871-879.

Batoz, J.L., and Dhatt, G. (1979). "Incremental displacement algorithms for nonlinear problems," International Journal of Numerical Methods in Engineering, vol 14, no. 8, 1979, pp 1262-1267.

Crisfield, M.A. (1981). "A fast incremental/iterative solution procedure that handles snap-through," Computers and Structures 13, 1981, pp 55-62.

Curtiss, Gary N. (1983). Structural analysis field investigation, South Pole, Noble, Inc., 120 East Ocean Blvd., Long Beach, CA 90802, 27 Apr 1983.

Engineering News-Record (1969). Dome will be home at South Pole. Nov 1969.

Gould, P.L. (1985). Finite element analysis of shells of revolution. Marshfield, MA, Pittman Publishing, Inc., 1985.

Haisler, W.E., Stricklin, J.A., and Key, J.E. (1977). "Displacement incrementation in non-linear structural analysis by the self-correcting method," International Journal of Numerical Methods in Engineering, vol 11, 1977, pp 3-10.

Jagannathan, D., Epstein, H., and Christian, P. (1975). "Nonlinear analysis of reticulated space trusses," Journal of the Structural Division, ASCE, vol 101, no. ST12, Dec 1975, pp 2641-2658.

Key, S.W., Stone, C.M., and Krieg, R.D. (1981). "A solution strategy for the quasi-static, large deformation, inelastic response of axisymmetric solids," in Nonlinear Finite Element Analysis in Structural Mechanics, W. Wunderlich et al., Eds., Springer-Berlin, New York, N.Y., 1981, pp 585-620.

Lunsford, Katherine (1987). South Pole Station monitoring program-procedures and results. Letter Report NCEL, 14 Aug 1987, Ser L61/1487, Naval Civil Engineering Laboratory, Port Hueneme, CA.

Mullord, P. (1984). "A review of collapse analysis of space structures," in Proceedings of the Third International Conference on Space Structures, H. Nooshin, Ed., Elsevier Applied Science Publishers, London, England, Sep 1984, pp 647-649.

Oran, C. (1973). "Tangent stiffness in space frames," Journal of the Structural Division, ASCE, 99 (ST6), 1973, pp 987-1001.

Papadrakakis, M. (1981). "Post-buckling analysis of spatial structures by vector iteration methods," Computers and Structures, 14, 1981, pp 393-402.

Pfluger, A. Elementary statics of shells, 2nd Ed, New York, N.Y., McGraw-Hill Book Company, 1961.

Powell, G., and Simons, J. (1981). "Improved iteration strategy for nonlinear structures," International Journal of Numerical Methods in Engineering, vol 17, 1981, pp 1455-1467.

Ramm, E. (1981). Strategies for tracing nonlinear responses near limit points," in Nonlinear Finite Element Analysis in Structural Mechanics, Wunderlich et al., Eds., Springer-Verlag, New York, N.Y., 1981, pp 63-89.

Rheinboldt, W.C., and Riks, E. (1983). "Solution techniques for nonlinear finite element equations," Chapter 7, State-of-the-Art Surveys on Finite Element Technology, A.K. Noor and W.D. Pilkey, Eds., ASME, New York, NY, 1983.

Riks, E. (1972). "The application of Newton's method to the problem of elastic stability," Journal of Applied Mechanics, vol 39, 1972, pp 1060-1066.

Riks, E. (1984). "Bifurcation and stability, a numerical approach," in Proceedings of the International Conference on Innovative Methods for Nonlinear Problems, New Orleans, LA, Lui, Belytscho, and Park, Eds., Pineridge Press International, Ltd., 1984, pp 313-344.

Shugar, T.A., Holland, T.J., Johnson, F.R., and Shoemaker, N.F. (1987). Preliminary analysis for predicting collapse of the South Pole Dome due to foundation settlement," Naval Civil Engineering Laboratory, TM-51-87-03, Port Hueneme, CA, Feb 1987.

Shugar, T.A. and Holland, T.J. (1987). "Lattice dome collapse prediction due to settlement," in Proceedings, Building Structures, Orlando, FL, ASCE Structures Congress, Donald R. Sherman, Ed., 1987, 17-20 Aug 1987, pp 332-343.

Simons, J.W., and Powell, G.H. (1982). "Solution strategies for statically loaded nonlinear structures," Earthquake Engineering Research Center, UCB/EERC-82/22, Nov 1982.

Task Committee on Latticed Structures (1976). "Latticed structures: State-of-the-art report." Journal of the Structural Division, ASCE, ST11, Nov 1976, pp 2197-2230.

Temcor (1969). Temcor polyframe geodesic dome, erection manual. Contract No. N62578-69-C-0130, Temcor, 2825 Toledo St., Torrance, CA, 90503, 1 Dec 1969.

Tezcan, S.S., and Ovune, B. (1966). "An iteration method for the nonlinear buckling of framed shells," Space Structures, R.M. Davies, Ed., London, England, 1966.

Tezcan, S.S. (1966). "Computer analysis of plane and space structures," Journal of the Structures Division, ASCE, vol 92, ST2, 1966, pp 143-173.

Timoshenko, Stephen P., and Woinowsky-Krieger, S. (1959). Theory of plates and shells, 2nd Ed. New York, NY, McGraw-Hill, 1959.

Underwood, P. (1983). "Dynamic relaxation," Chapter 5, Computational Methods for Transient Analysis, T. Belytschko and T.J.R. Hughes, Eds., Elsevier Science Publishers B.V., Amsterdam, 1983.

Zhao, H.L., et al. (1984). "Experimental study, theoretical analysis and design of a sheet-framed space structure," in Proceedings of the Third International Conference on Space Structures, H. Nooshin, Ed., Elsevier Applied Science Publishers, London, England, Sep 1984, pp 219-224.

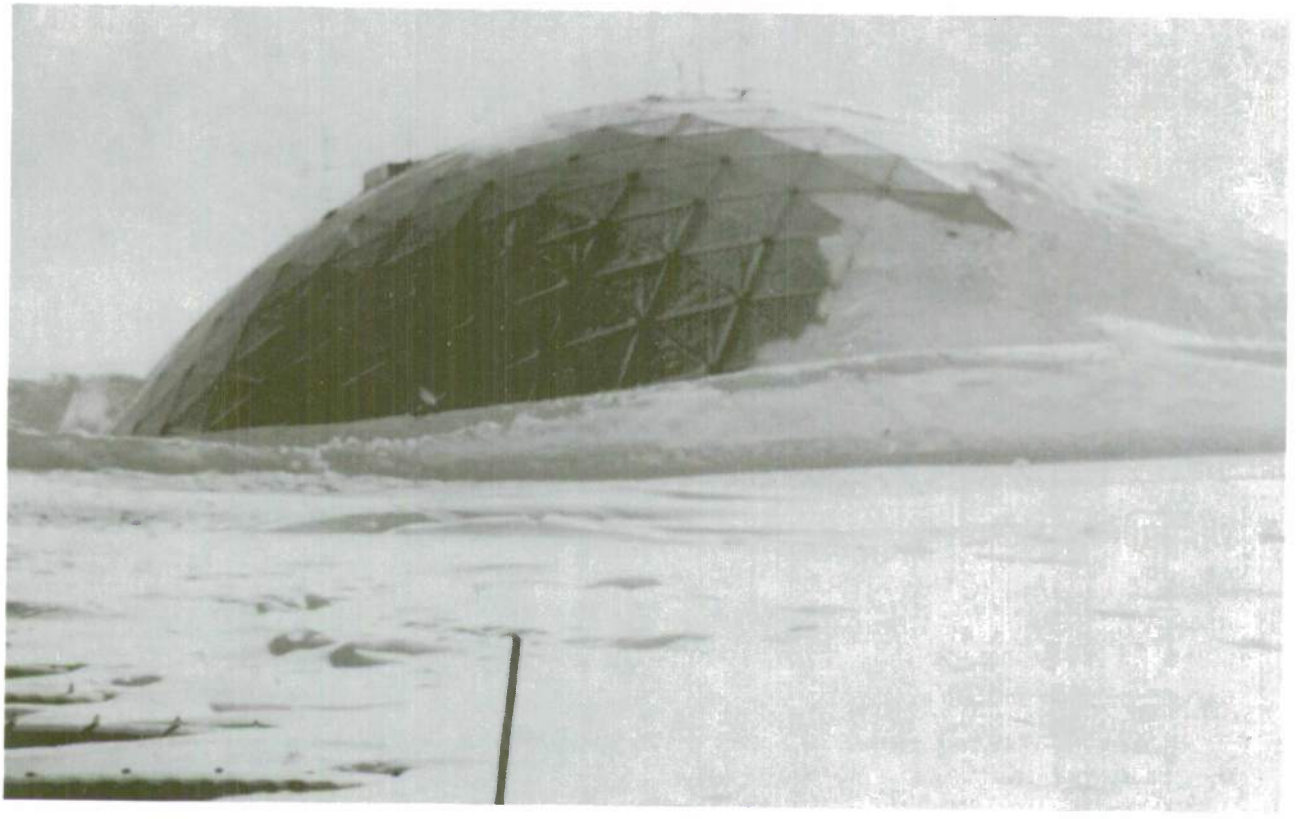

Figure 1. South Pole Dome.

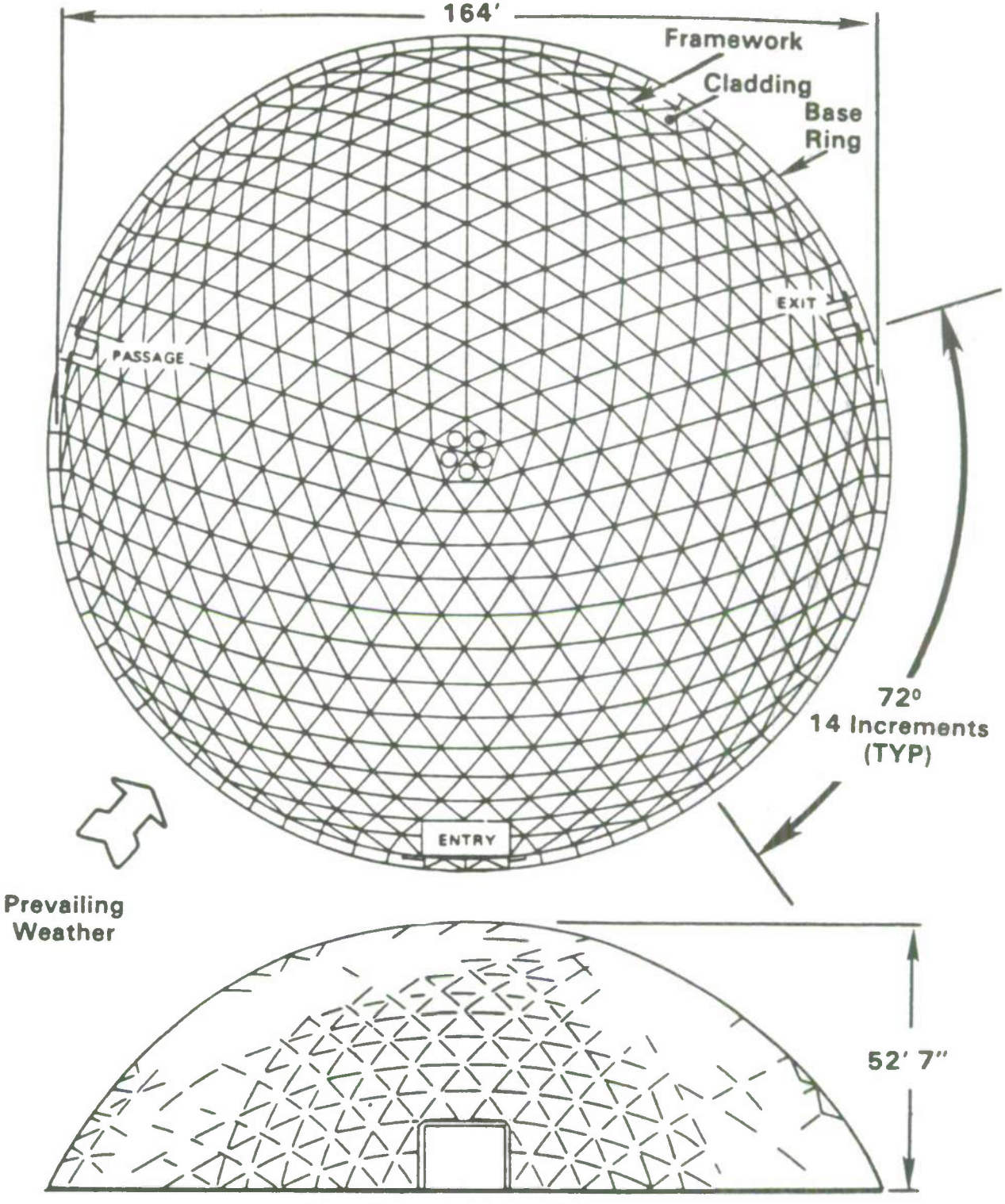

(a) Elevation and plan views.

Figure 2. Overall configuration of South Pole Dome (after Temcor, 1969).

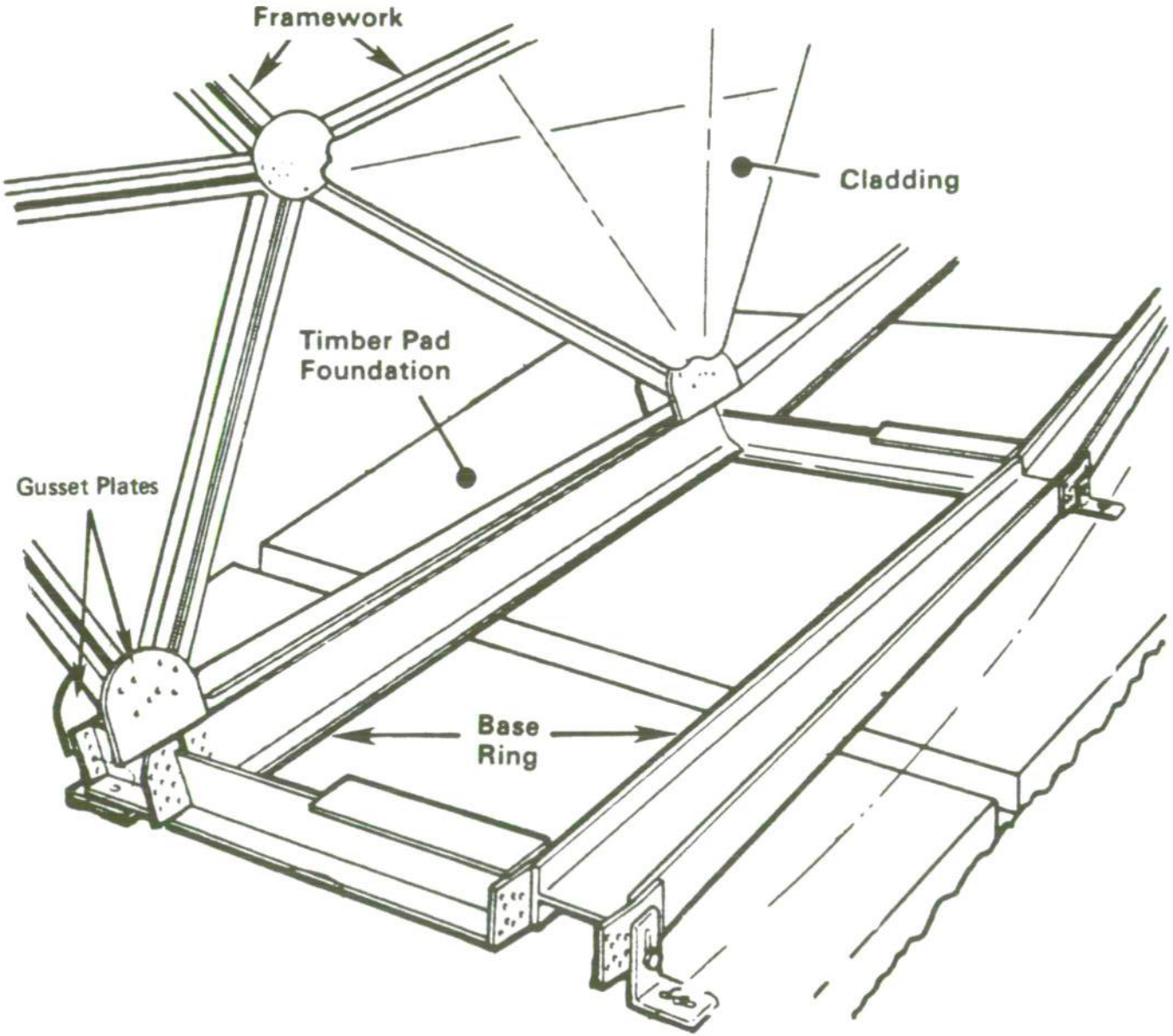

(b) Base ring and foundation.

Figure 2. Continued.

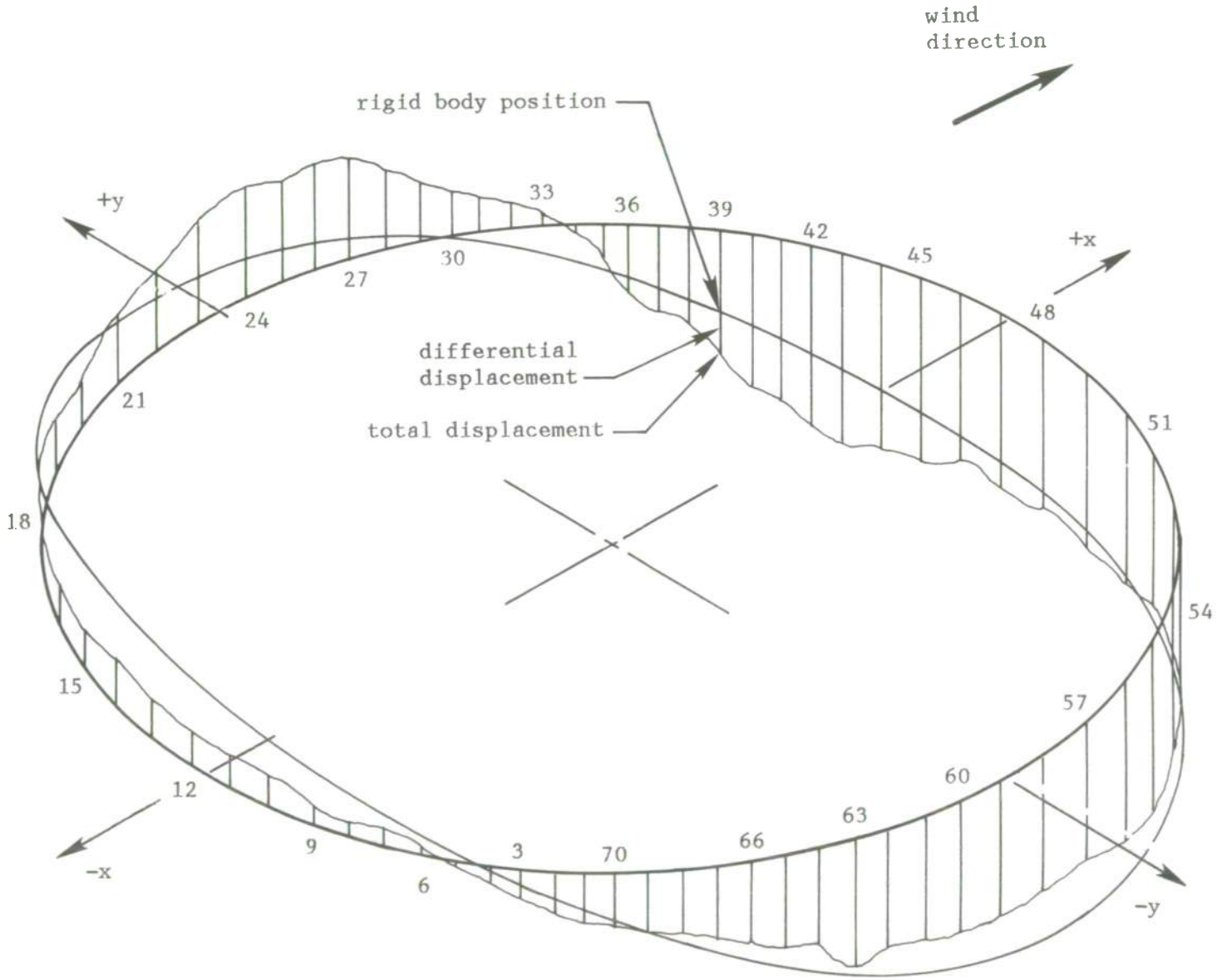

Figure 3. Differential displacement of dome foundation.

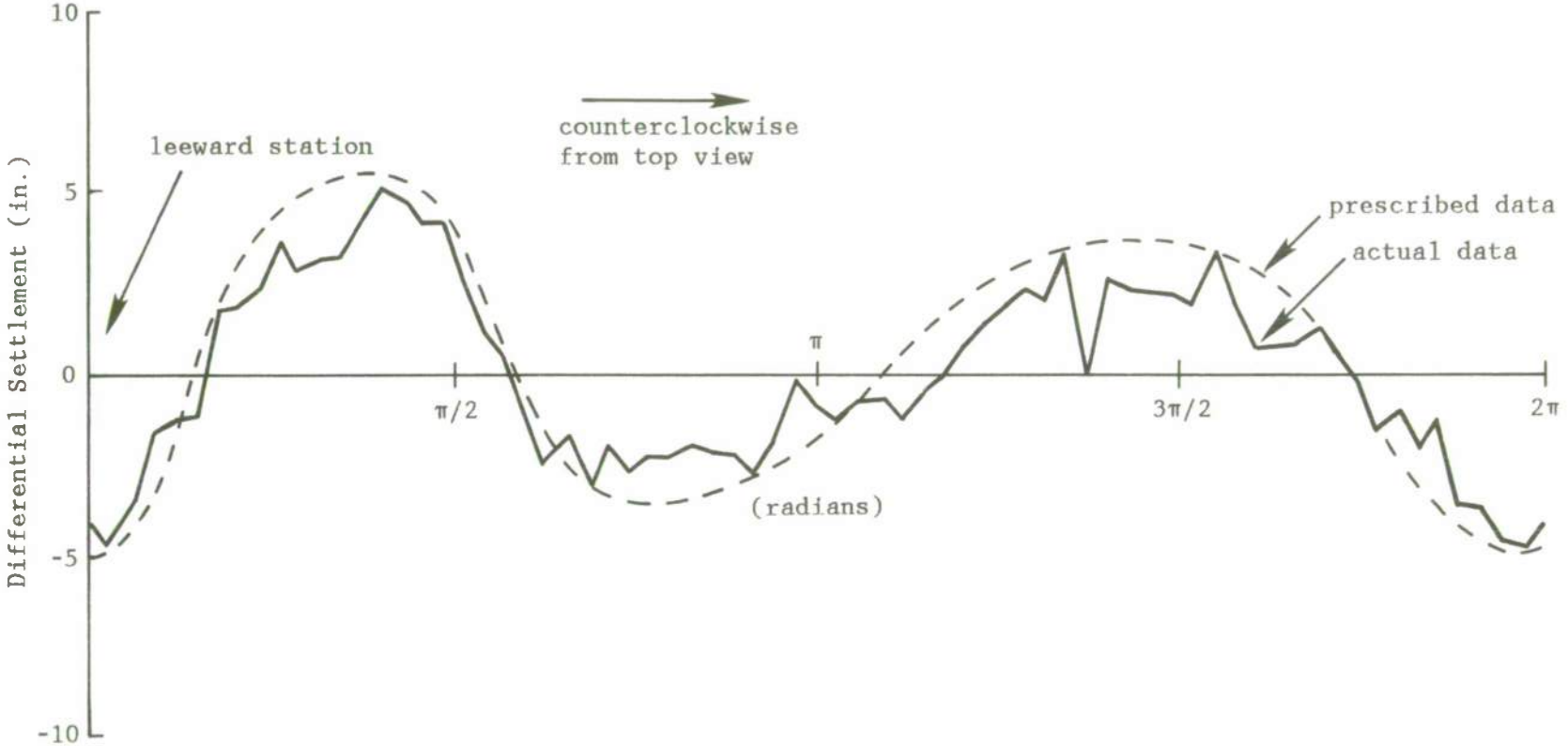

Figure 4. Differential settlement of South Pole Dome base ring.

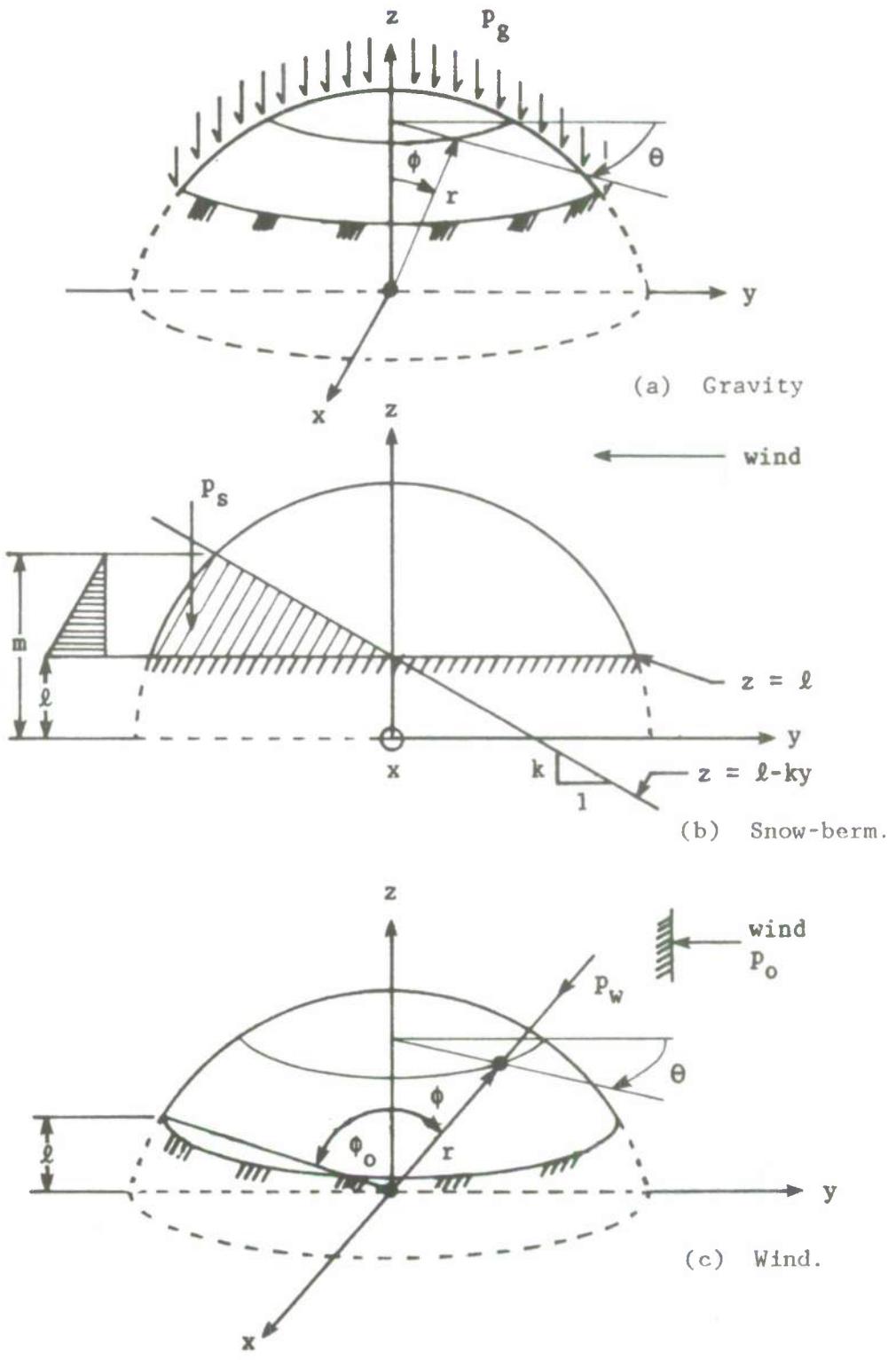

Figure 5. Conventional loads.

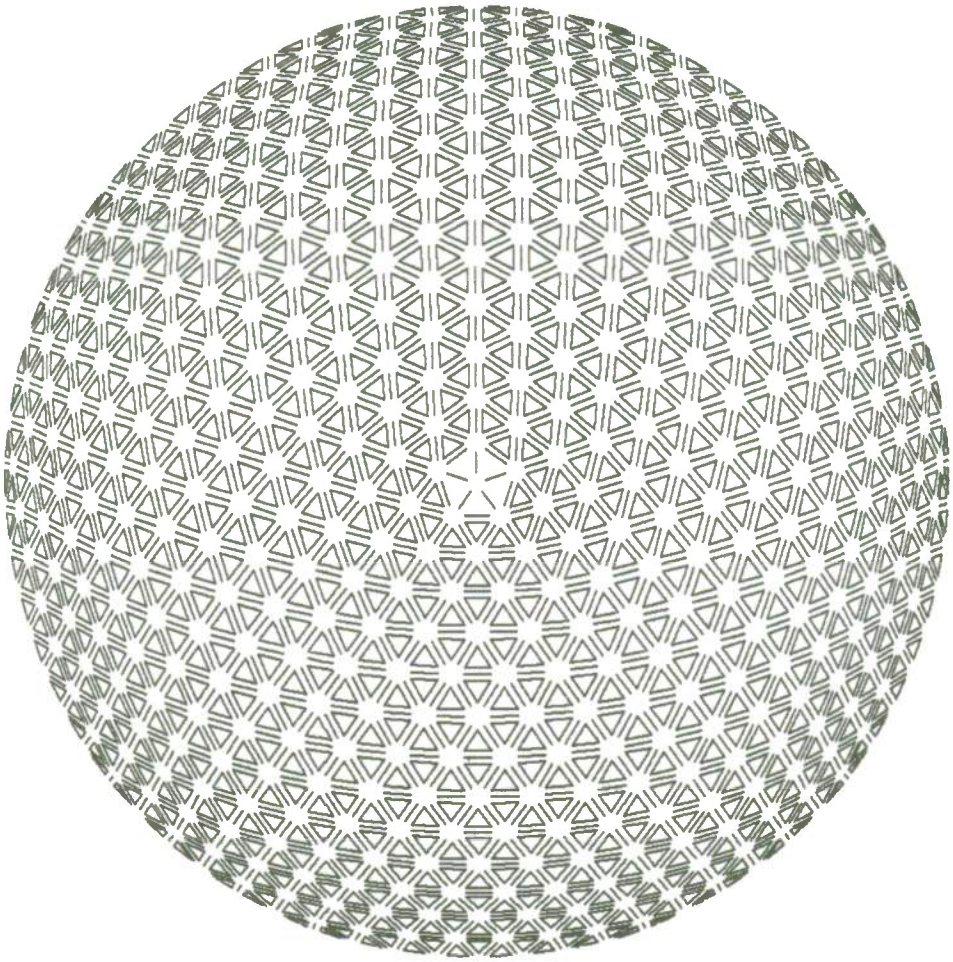

(a) Plan.

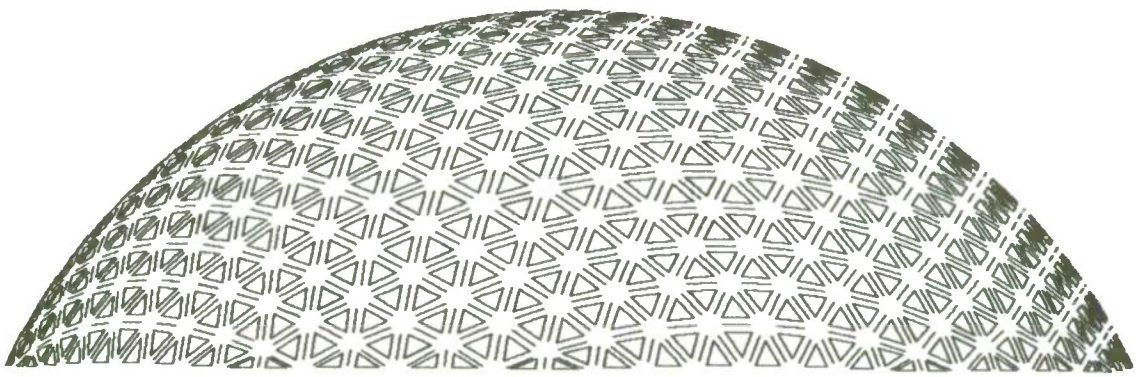

(b) Elevation.

Figure 6. South Pole Dome finite element topology and geometry.

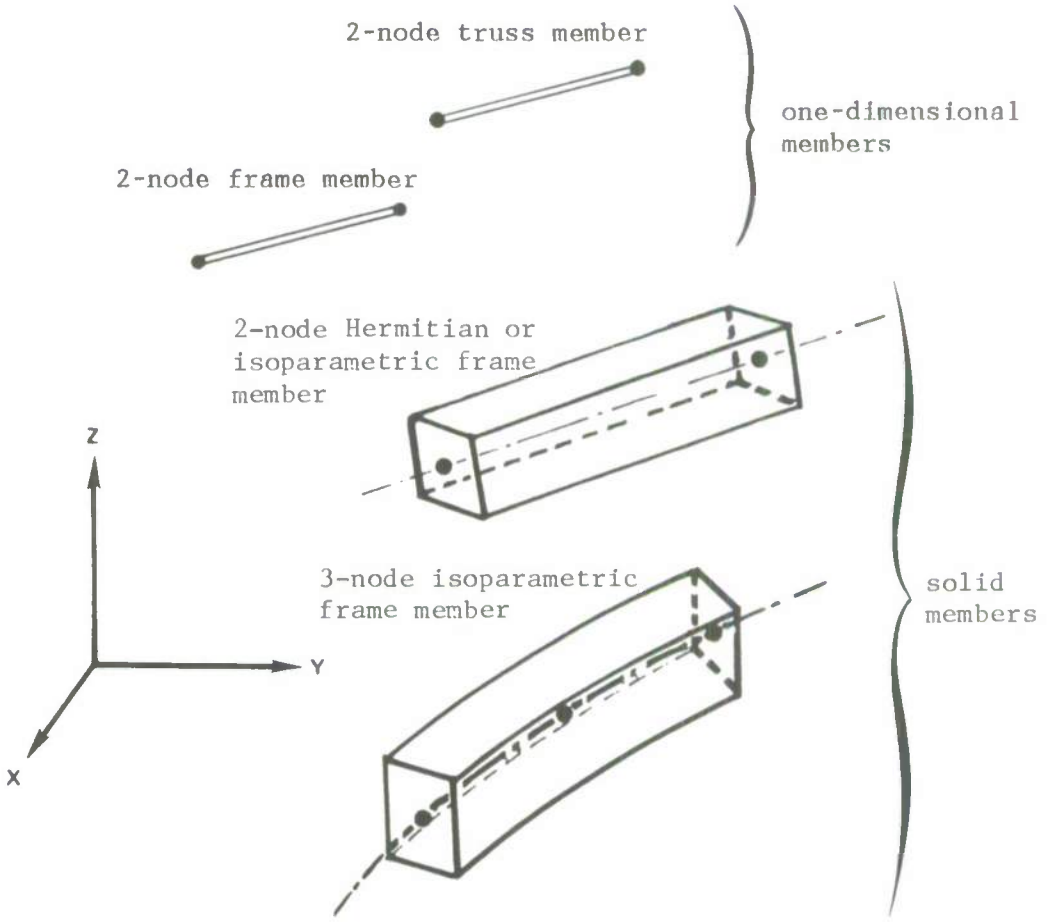

Figure 7. Candidate finite element models for latticed dome framework.

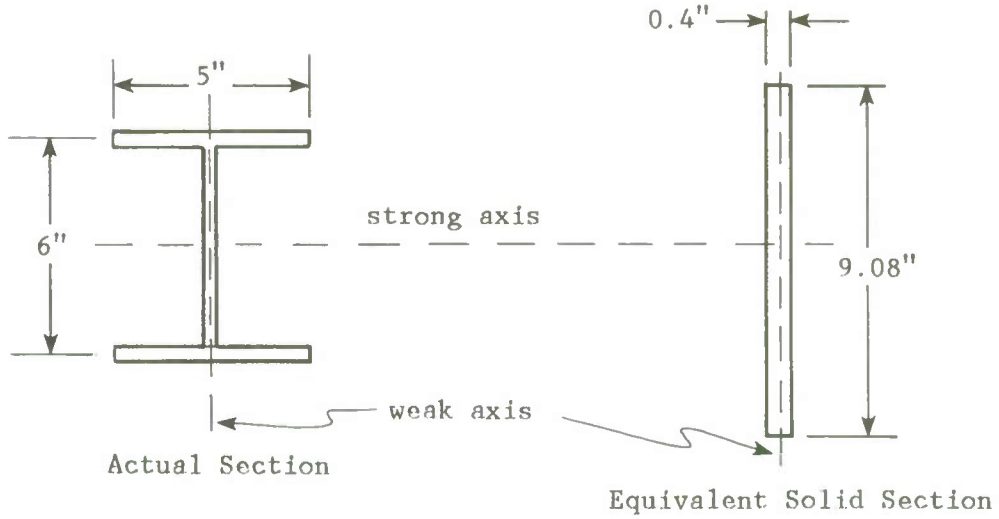

(a) Frame member.

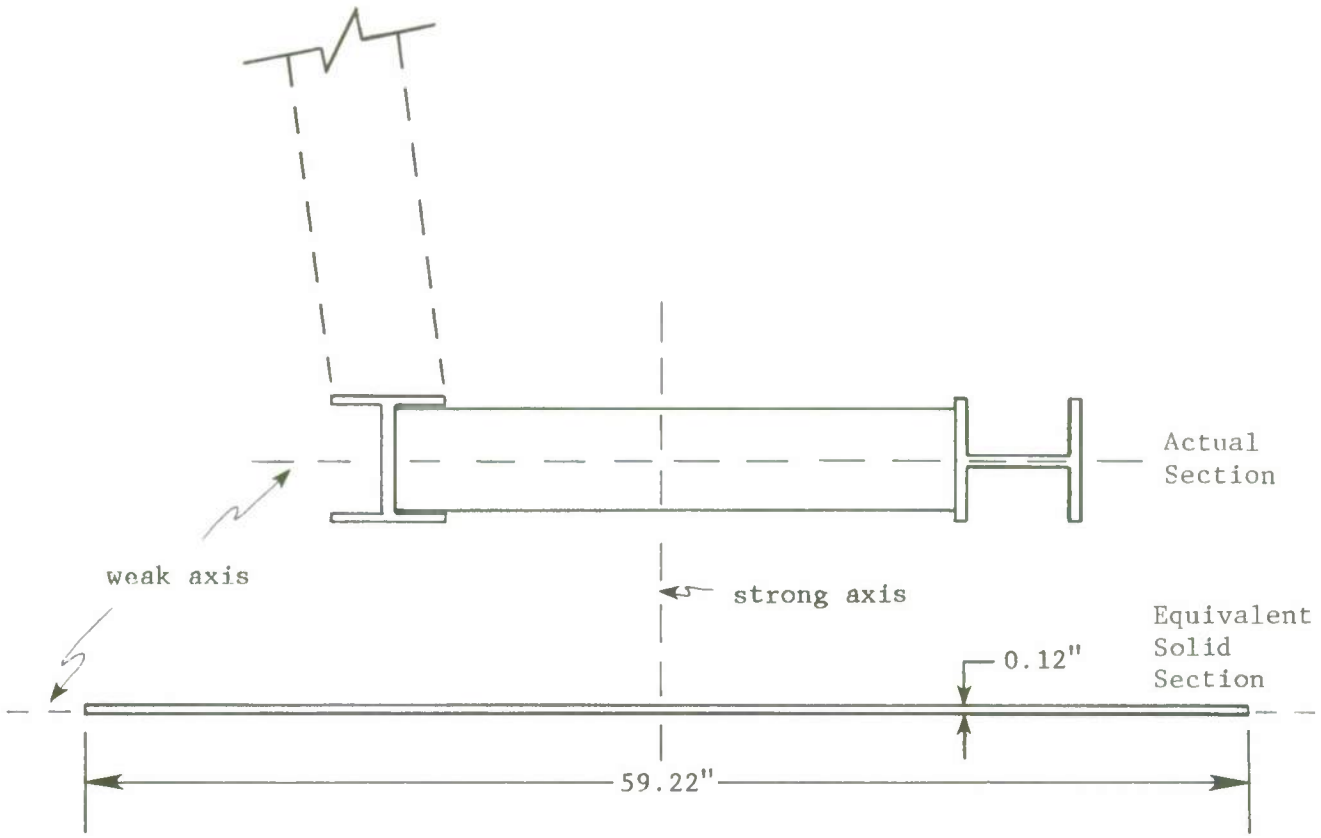

(b) Base ring.

Figure 8. Geometry of actual and equivalent sections for the South Pole Dome.

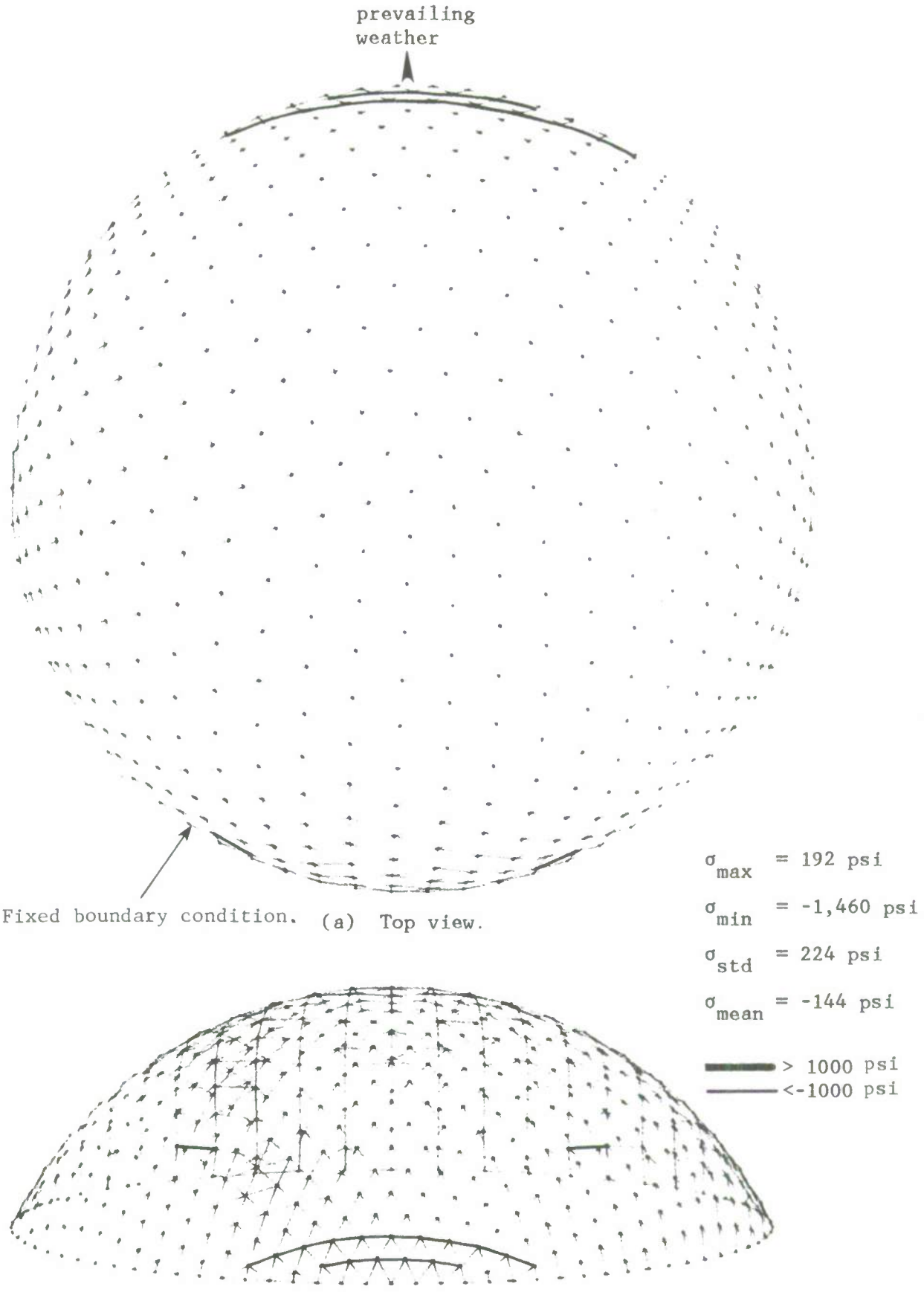

Figure 9. Member stresses due to snow-berm load - linear analysis results.

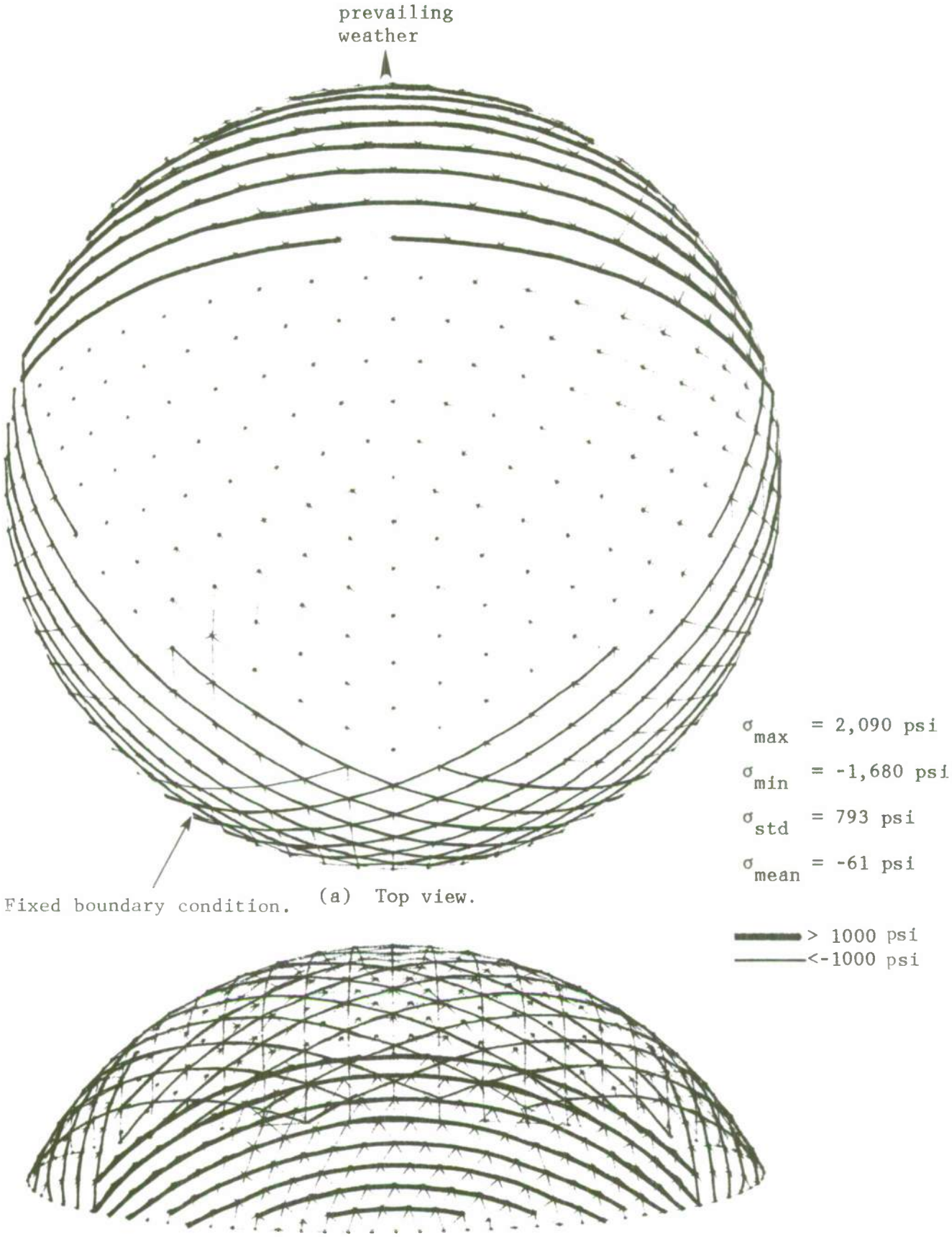

(b) Wind direction view.

Figure 10. Member stresses due to full wind loading - linear analysis results.

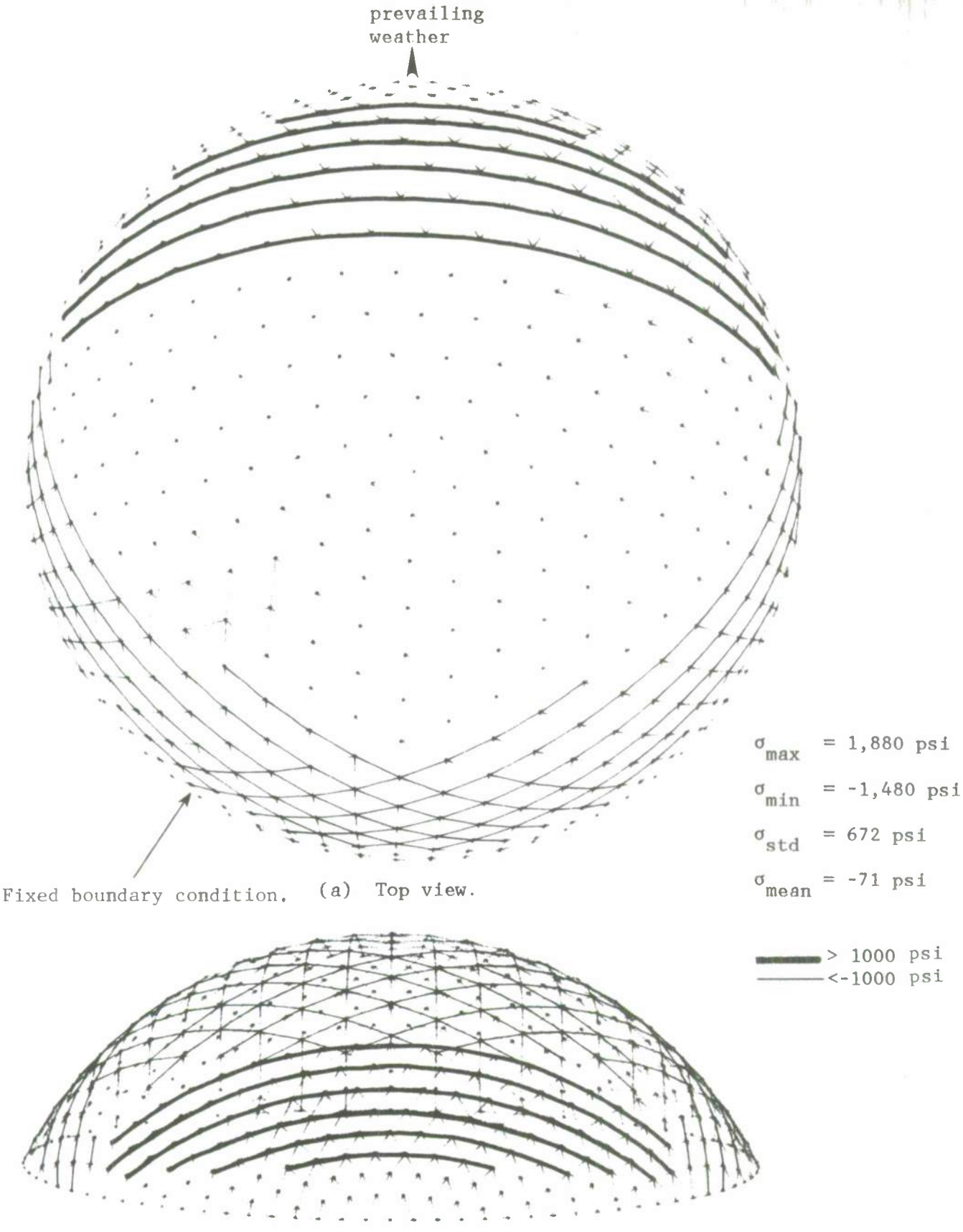

Figure 11. Member stresses due to partial wind loading - linear analysis results.

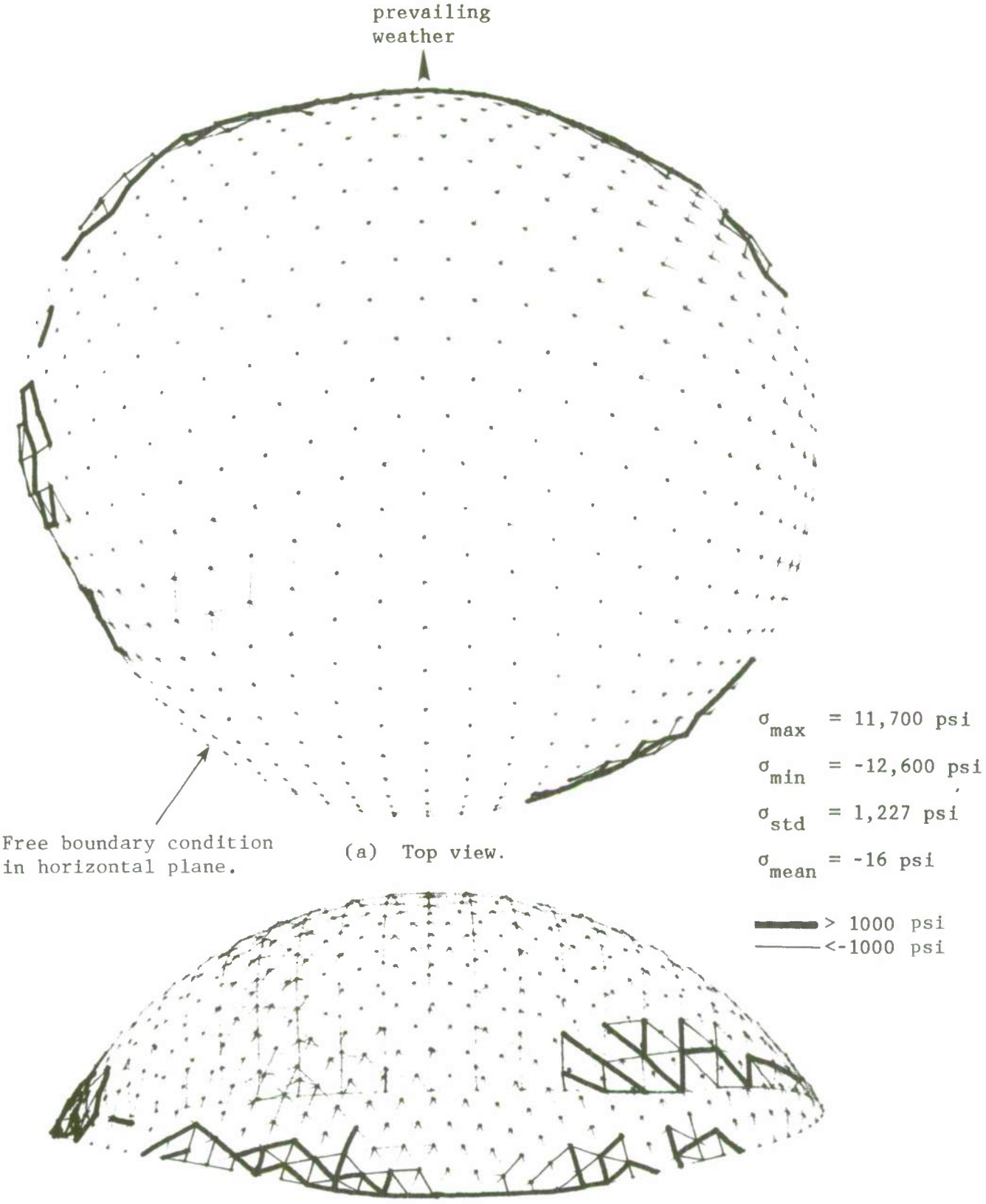

Figure 12. Member stresses and settlement displacements - linear analysis results.

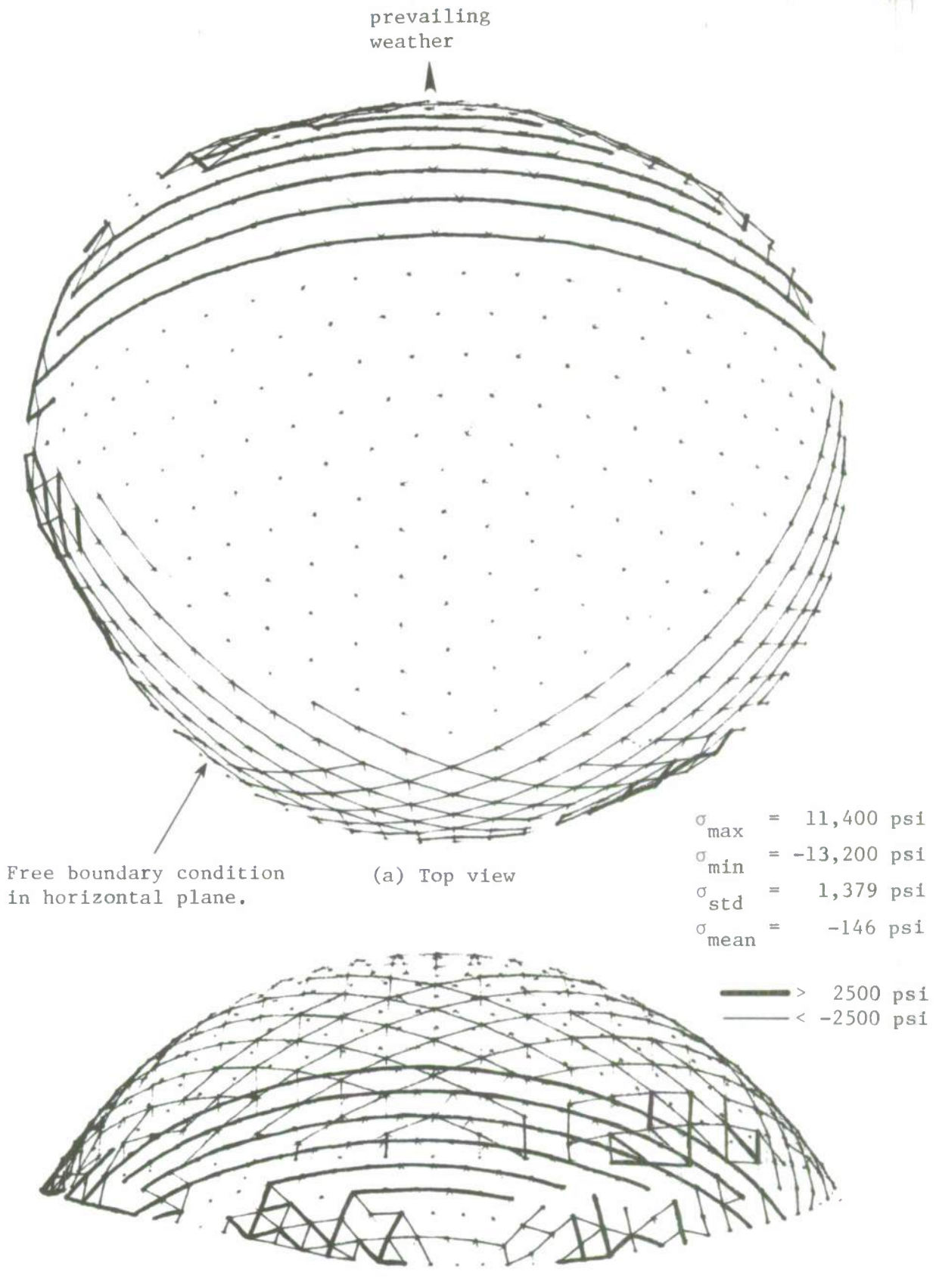

(b) Wind direction view.

Figure 13. Member stresses and settlement displacements for combined loading - linear analysis results.

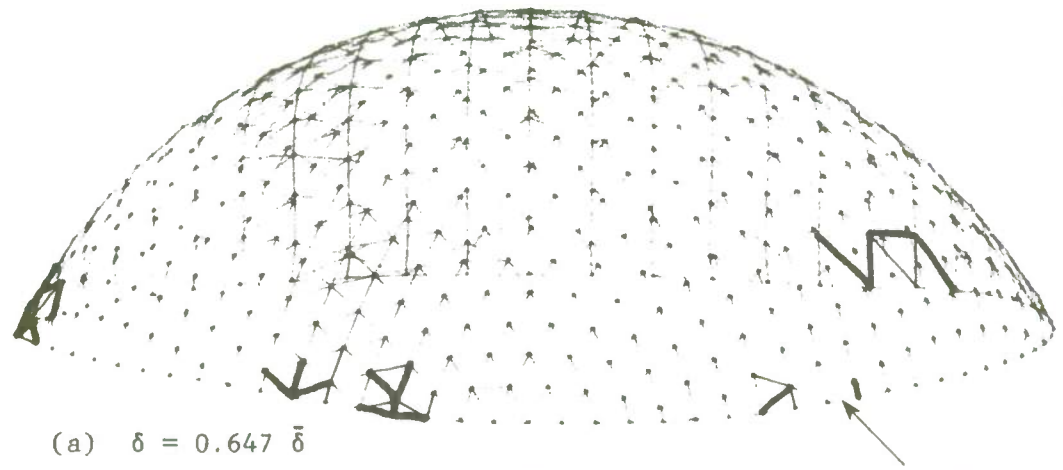

> 2500 psi
<-2500 psi

σ_{max} = 7,790 psi
σ_{min} = -8,200 psi
σ_{std} = 789 psi
σ_{mean} = 1 psi

(a) $\delta = 0.647\ \bar{\delta}$

Free boundary condition in horizontal plane.

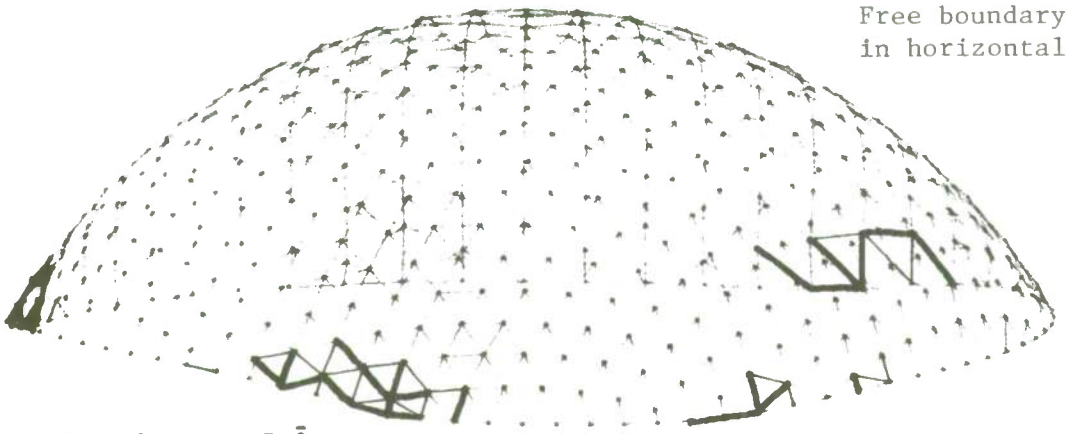

σ_{max} = 13,300 psi
σ_{min} = -14,000 psi
σ_{std} = 1,335 psi
σ_{mean} = 2 psi

(b) $\delta = 1.095\ \bar{\delta}$

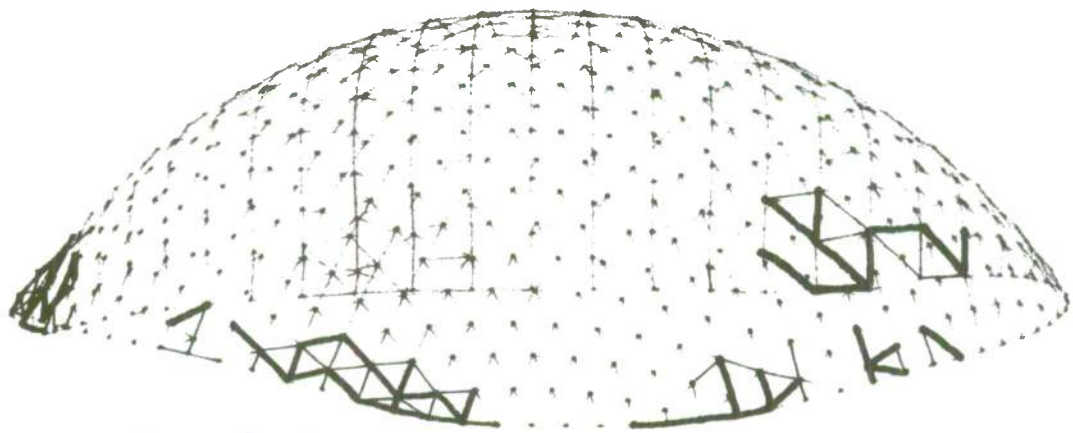

σ_{max} = 19,000 psi
σ_{min} = -19,900 psi
σ_{std} = 1,884 psi
σ_{mean} = 8 psi

(c) $\delta = 1.544\ \bar{\delta}$

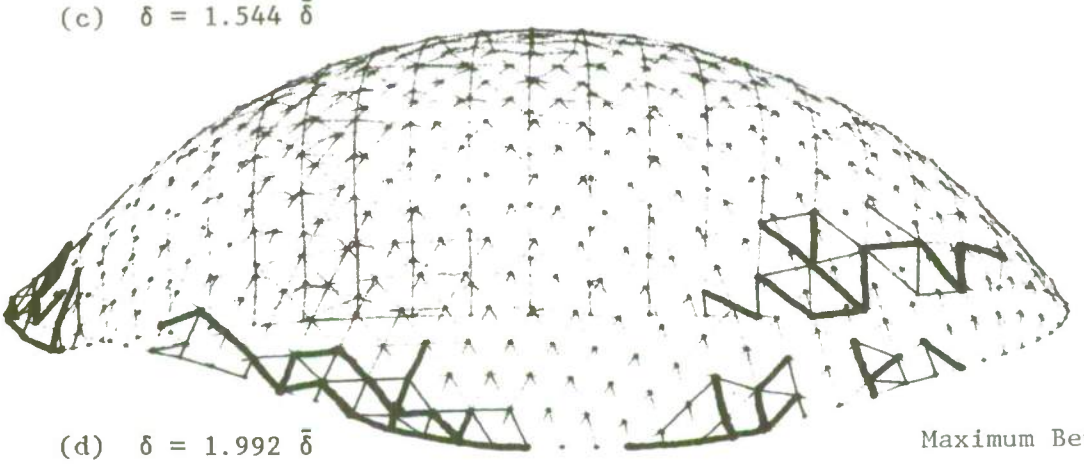

σ_{max} = 24,700 psi
σ_{min} = -25,800 psi
σ_{std} = 2,435 psi
σ_{mean} = 45 psi

(d) $\delta = 1.992\ \bar{\delta}$

Maximum Bending Stress $\approx$ 100 psi

Figure 14. Member stresses and settlement displacements - nonlinear analysis results.

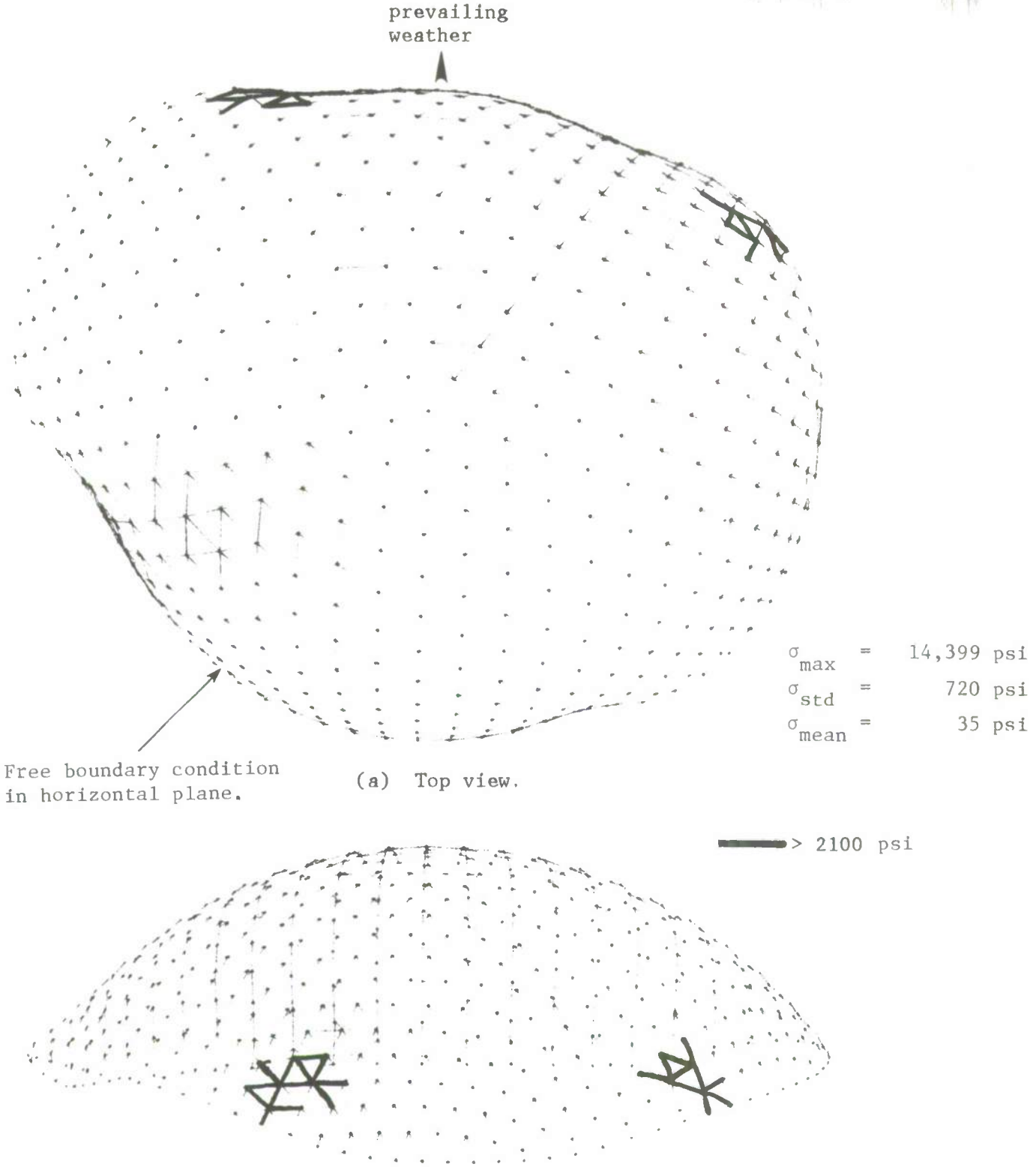

Figure 15. Bending stresses and settlement displacements - locally unstable configuration at $\delta = 2.194\ \bar{\delta}$.

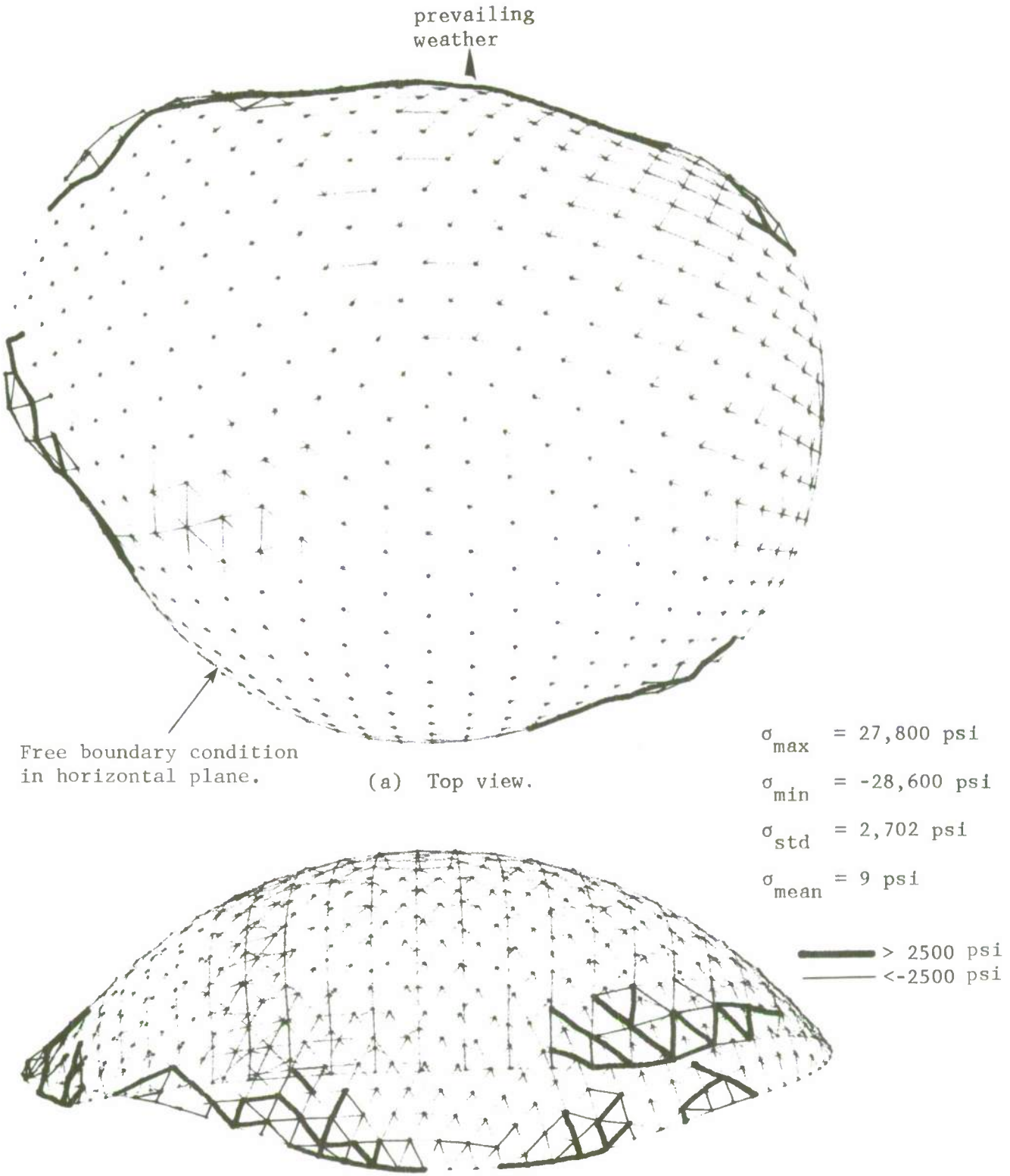

Figure 16. Axial stresses and settlement displacements - locally unstable configuration at $\delta = 2.194\ \bar{\delta}$.

Appendix A

APPLICABLE SHELL MEMBRANE THEORY

The force intensities (force per unit length) associated with the shell membrane theory are illustrated in Figure A-1 for a spherical dome configuration. Here N_ϕ is the meridional force, N_θ is the hoop force, and T is the in-plane shear force. The governing equilibrium equations for the shell membrane theory applied to the spherical dome, as given by Pfluger (1961), are as follows:

$$\frac{\partial}{\partial\phi}(N_\phi \sin\phi) + \frac{\partial T}{\partial\theta} - N_\theta \cos\phi + p_{x'} r \sin\phi = 0$$

$$\frac{\partial N_\theta}{\partial\theta} + \frac{\partial}{\partial\phi}(T \sin\phi) + T \cos\phi + p_{y'} r \sin\phi = 0$$

$$N_\phi + N_\theta + p_{z'} r = 0$$

The terms $p_{x'}$, $p_{y'}$ and $p_{z'}$ represent applied forces per unit area in the direction of the indicated axes. It is seen that when foundation distortion is the only load acting on the dome ($p_{x'} = p_{y'} = p_{z'} = 0$) that the hoop and meridian forces are equal and opposite in sign everywhere on the dome surface,

$$N_\theta = - N_\phi$$

Foundation settlement may be regarded as a disturbance of the membrane theory displacement solution causing disturbances to the membrane equilibrium solution. It is well known that disturbances of membrane equilibrium that are due to incompatibility with conditions of deformation at the boundaries are normally confined to a narrow zone in the vicinity of the disturbances. Further while in general, the membrane theory cannot satisfy the conditions of deformation compatibility, the error is negligibly small. According to Timoshenko (1959), for a

spherical dome of radius r and thickness h acted upon by gravity, the error in the maximum stress (which occurs at the crown) is dependent on the ratio h/r as follows:

$$\left[\frac{\text{bending stress}}{\text{membrane stress}}\right]_{max} \leq 3.29\ h/r$$

The ratio h/r for the South Pole Dome would be less than 0.005.

The membrane theory solution for gravity loading (see Figure 5a) is:

$$N_\theta = p_g\, r\left[\frac{1}{1 + \cos\phi} - \cos\phi\right]$$

$$N_\phi = p_g\, r\left[\frac{1}{1 + \cos\phi}\right]$$

$$T = 0$$

The membrane theory solution for wind load (see Figure 5c) is:

$$N_\theta = p_o \frac{r}{3} \frac{\cos\theta}{\sin^3\phi} (2\cos\phi - 3\sin^2\phi - 2\cos^4\phi)$$

$$N_\phi = -\,p_o \frac{r}{3} \frac{\cos\theta\cos\phi}{\sin^3\phi} (2 - 3\cos\phi + \cos^3\phi)$$

$$T = -\,p_o \frac{r}{3} \frac{\sin\theta}{\sin^3\phi} (2 - 3\cos\phi + \cos^3\phi)$$

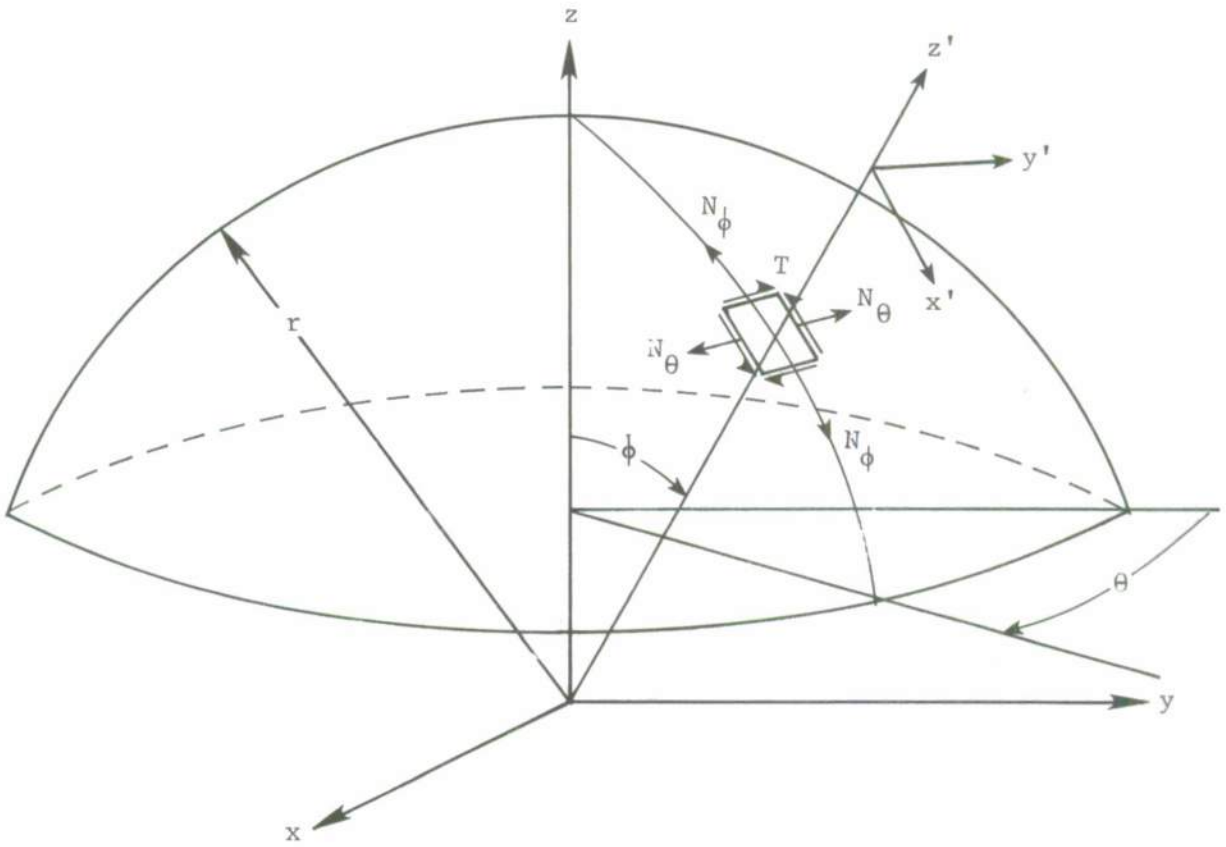

Figure A-1. Force intensity variables for membrane theory.

Appendix B

EFFECT OF RIGID JOINTS ON MODEL STIFFNESS

A typical idealized module of the South Pole Dome's framework was analyzed as both a space truss and a space frame. The model of this module is shown in Figure B-1. Dimensions and member sizes are as close as possible to actural values for the dome. The properties of the model are listed in Table B-1. The ADINA structural analysis program was used to perform this study, and linear behavior is assumed.

The results of the study are summarized in Table B-2. When members have bending stiffness, the structure's latteral stiffness, in direction 3, is increased by a factor of 5. However, the in-plane stiffness, in the 1- and 2-directions, is not affected by the addition of bending stiffness to the members. The in-plane stiffness is 50 times the lateral stiffness.

If loading is inplane (tangent to the dome's surface), then the truss model is adequate. Otherwise, for lateral loading (normal to the dome's surface), the dome must be modeled as a space frame to replicate accurate load-deflection behavior.

Table B-1. Properties of Module Model

E	10×10^{6} psi	6.90×10^{10} N/m^2
μ	0.3	0.3
A	3.66 in.^{2}	0.0024 m^2
L	98.5386 in.	2.50288 m
$I_{z'}$	25.11 in.^{4}	1.042×10^{-5} m^4
$I_{y'}$	5.86 in.^{4}	2.432×10^{-6} m^4
J	25.78 in.^{4}	1.070×10^{-5} m^4
r	78.5 in.	2.5 m
H	4.728 in.	0.12 m

Table B-2. Effect of Rigid Joints on Stiffness

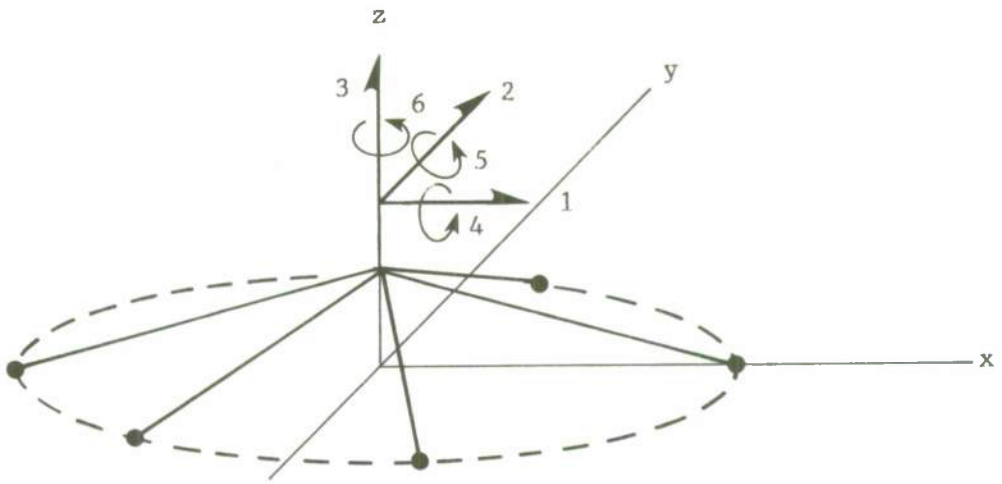

Space Truss Stiffness Matrix:

$$\underset{\sim}{K} = \begin{array}{c} \\ 1 \\ 2 \\ 3 \end{array} \begin{array}{c} \begin{array}{ccc} 1 & 2 & 3 \end{array} \\ \begin{bmatrix} 1.9804 & 0 & 0 \\ 0 & 1.9804 & 0 \\ 0 & 0 & 0.009 \end{bmatrix} \end{array} \times 10^{8} \text{N/m}$$

Space Frame Stiffness Matrix:

$$\underset{\sim}{K} = \begin{array}{c} \\ 1 \\ 2 \\ 3 \\ 4 \\ 5 \\ 6 \end{array} \begin{array}{c} \begin{array}{cccccc} 1 & 2 & 3 & 4 & 5 & 6 \end{array} \\ \begin{bmatrix} 1.9842 & 0 & 0 & 0 & -0.0012 & 0 \\ 0 & 1.9842 & 0 & 0.0012 & 0 & 0 \\ 0 & 0 & 0.0420 & 0 & 0 & 0 \\ 0 & 0.0012 & 0 & 0.0379 & 0 & 0 \\ -0.0012 & 0 & 0 & 0 & 0.0379 & 0 \\ 0 & 0 & 0 & 0 & 0 & 0.0161 \end{bmatrix} \end{array} \times 10^{8} \text{N/m}$$

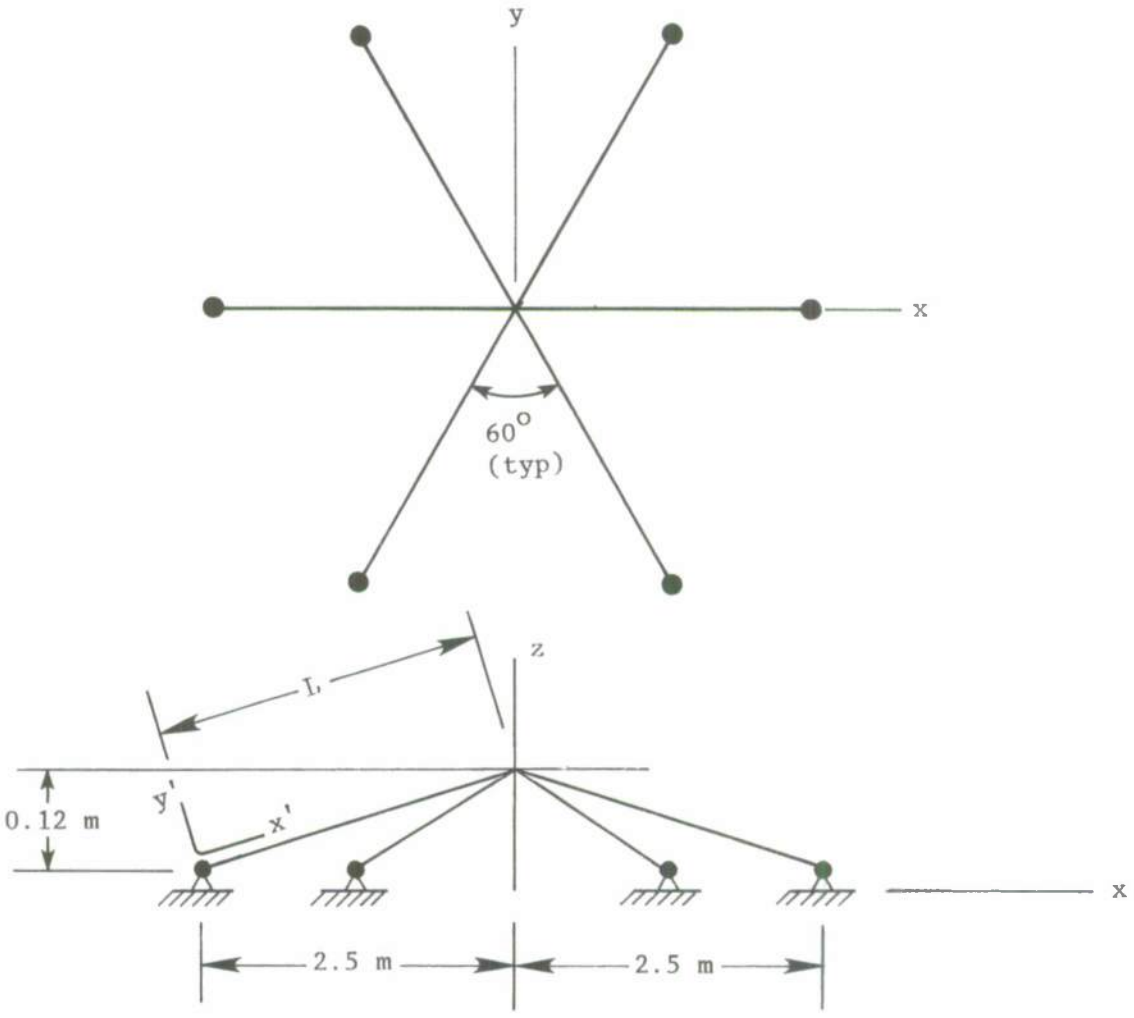

Figure B-1. South Pole Dome module model.

Appendix C

COMPARISON OF ONE-DIMENSIONAL AND SOLID FRAME ELEMENTS

It is not emphasized often enough in structural analysis by computer methods that three-dimensional solid frame finite elements have a serious limitation in being incapable of modeling all the section properties of frame members possessing other than rectangular or circular sections. Thus, for all its advantages, the solid frame element cannot accurately model the behavior of frame elements subjected to combined action; axial, biaxial bending, and torsion when biaxial bending and torsion are important.

In specifying the width and depth of a solid rectangular section, the analyst can only capture two of the four section properties of a frame member. For example, the cross-section area and the major inertia of the section can be accurately replicated, but corresponding values of the minor inertia and torsional constant of the section will, in general, be inaccurate.

The alternative, one-dimensional frame element, does not have this disadvantage because all four section properties (area, maximum and minimum moments of inertia, and torsional constant) are directly prescribed when using in these elements.

Advantages of solid frame finite elements applied to rectangular or circular sections include:

1. Curved members can be modeled easily.
2. Extension to nonlinear material behavior is straight forward.
3. Tapered members can be modeled easily.
4. Shear deformation are included easily.

On the other hand, the above features require special handling techniques to implement with one-dimensional frame elements. In these elements pre-integration through the depth and width of the section, assuming Bernoulli beam theory behavior, has foreclosed on the special considerations listed above.

To verify correct behavior of the solid frame finite element, the South Pole Dome member module (see Appendix B) was modeled with this element. The member section properties prescribed for the model were the equivalent properties listed in Table 2 of the report. The ADINA program was used to calculate the stiffness matrix for this model. This matrix is shown in Table C-1, and it should be compared with that in Table B-2. It is seen that the ADINA solid frame finite element is within 2.2 percent of the one-dimensional frame element regarding tangential stiffness and within less than 1 percent regarding normal stiffness of the South Pole Dome member module.

Thus, in spite of the inability of the solid frame finite element to model all section properties accurately, it should behave satisfactorily in replicating the South Pole Dome load-deflection behavior.

Table C-1. Frame Stiffness Matrix

$$\underset{\sim}{K} = \begin{bmatrix} 1.9409 & 0 & 0 & 0 & -0.0010 & 0 \\ 0 & 1.9409 & 0 & 0.0010 & 0 & 0 \\ 0 & 0 & 0.0419 & 0 & 0 & 0 \\ 0 & 0 & 0 & 0.0372 & 0 & 0 \\ 0 & 0 & 0 & 0 & 0.0372 & 0 \\ 0 & 0 & 0 & 0 & 0 & 0.0001 \end{bmatrix} \times 10^{8} \text{N/m}$$

Appendix D

EFFECT OF CLADDING ON MODEL STIFFNESS

To determine the effect of the South Pole Dome's cladding on the load-deflection behavior of the Dome, the cladding for the member module (see Appendix B) was modeled by six triangular plate finite elements. Two different plate element formulations, both available in the general purpose program ADINA, were investigated; a four-node element with two adjacent nodes coalesced to form a triangle, and a three-node, discrete Kirchhoff element (see Bathe, 1982). The plate elements were added to the member module framework which was modeled by the solid frame finite elements discussed in Appendix C.

The computed stiffness matrices for the South Pole Dome member module including the effect of cladding, are presented in Table D-1 for both plate elements studied. These matrices should be compared with the stiffness matrix presented in Table C-1 which neglects the effect of cladding. The addition of the cladding increases the tangential stiffness of the South Pole Dome module by a factor of 2. The normal stiffness is increased by a factor of 29 using the 4-node plate element, and by a very different factor of 1.24 using the 3-node discrete Kirchhoff plate element. The latter result is a much more reasonable increase in stiffness considering the cladding is only 0.050 inch thick and the supporting frame members are 6 inches deep.

Based upon this study, the 3-node, discrete Kirchhoff plate finite element was used to model the cladding in the South Pole Dome structural analysis model.

Table D-1. Effect of Cladding on Stiffness

Stiffness matrix using 4-node plate elements:

$$\underset{\sim}{K} = \begin{bmatrix} 4.1842 & 0 & 0 & 0 & -0.0359 & 0 \\ 0 & 4.1842 & 0 & 0.0359 & 0 & 0 \\ 0 & 0 & 1.2143 & 0 & 0 & 0 \\ 0 & 0 & 0 & 0.7983 & 0 & 0 \\ 0 & 0 & 0 & 0 & 0.7983 & 0 \\ 0 & 0 & 0 & 0 & 0 & 0.0006 \end{bmatrix} \times 10^8 \text{ N/m}$$

Stiffness matrix using 3-node plate elements:

$$\underset{\sim}{K} = \begin{bmatrix} 4.1840 & 0 & 0 & 0 & -0.0010 & 0 \\ 0 & 4.1840 & 0 & 0.0010 & 0 & 0 \\ 0 & 0 & 0.0521 & 0 & 0 & 0 \\ 0 & 0 & 0 & 0.0378 & 0 & 0 \\ 0 & 0 & 0 & 0 & 0.0378 & 0 \\ 0 & 0 & 0 & 0 & 0 & 0.0002 \end{bmatrix} \times 10^8 \text{ N/m}$$

Appendix E

OVERVIEW OF COMPUTATIONAL METHODS FOR POST-BUCKLING ANALYSIS

The external load of a structural system that produces excessive deformations at the joints is defined as the buckling load. The buckling load can be calculated by either a linear or a nonlinear analysis. In the former approach, the geometric or initial stress matrix is superimposed onto the linear stiffness matrix, and the condition that buckling corresponds to the determinant of this combined matrix being zero is used to calculate the linear buckling load. In the latter approach, the member force-deformation relations consider the current or deformed configuration of the structure. This configuration is updated during the solution procedure for the buckling load. Though the linear approach can sometimes give satisfactory buckling load estimates, the nonlinear approach is more accurate when, as the external loads approach the buckling stage, the changes in geometry of the structure are very significant, i.e., when the structure is behaving nonlinearly. Tezcan and Ovune (1966) and Tezcan (1966) discuss the importance of nonlinear behavior and describe the corresponding nonlinear member force-displacement relationships for calculating the buckling load of framed shells. They did not address post-buckling behavior. During this early period of development in computational methods, it was considered sufficient enough to calculate the buckling load accurately.

Before reviewing the mainstream methods for calculating post-buckling behavior of structures which are based on Newton-type linearizations, the alternative, purely iterative, dynamic relaxation method should be mentioned.

The main drawback of the Newton-type linearization is its considerable computational effort in calculating the (approximate) tangent stiffness matrix on each iteration. There is also a difficulty in surpassing critical points, without auxiliary load step control calculations, where the tangent stiffness matrix becomes singular.

Papadrakakis (1981) has demonstrated an automated dynamic relaxation method that can trace the complete load-deflection path using displacement increments and can easily overcome critical points. The basic method is easy to implement. Only the relatively simple truss and frame member force-displacement relations, as given by Oran (1973) or Jagannathan et al. (1975) for example, are needed. Formulation of the tangent stiffness matrix is not required. The unbalanced forces at the joints which are used in calculating the residual force vector iterate are obtained from conditions of static equilibrium at each joint.

The dynamic relaxation method is an explicit method for the static solution of linear or nonlinear structural mechanics problems. It is based on the fact that the static solution is the steady state part of the transient response to a step load. The method is especially attractive for problems with highly nonlinear behavior which includes limit points or regions of very soft stiffness characteristics. All quantities are treated as vectors, and the method has low storage requirements. It is also referred to as a vector iteration method because it

requires no square matrix storage or formation. It requires very large numbers of iterations, but it also exhibits a tenacious ability to converge to the global solution (Shugar (1987)). The combination of simplicity and tenacity result in an efficient solution method for highly nonlinear problems. If the definition of robustness implies overall analysis efficiency, this method appears very robust, particularly the adaptive or automatic versions by Papadrakakis and by Underwood (1983). The method has consistently produced good results with no tendency to overshoot the solution, which is desirable when seeking solutions to buckling problems. Key et al. (1981) have successfully used this method for large complex nonlinear finite element analyses.

Perhaps for historical reasons, the majority of general purpose nonlinear finite element computer programs employ the Newton-type linearization methods for computing the buckling loads of structures. To calculate the post-buckling behavior, these programs use a form of load step control. The writers are aware of no general purpose programs that provide an option for using the dynamic relaxation solution method to solve this highly nonlinear problem.

In post-buckling analysis, it is well known that load incrementation breaks down near a critical point on the load-deflection path. For example, Jagannathan et al. (1975) reported, while using a Newton-type linearization method, that numerical instability occurred during the incremental/itertive solution process and that it was detected by a rapidly increasing residual norm. In the past 10 to 15 years, much research has been devoted to developing various methods of load step control to overcome numerical instability and compute post-buckling behavior.

One type of adaptive load adjustment technique is called a displacement control method. This method prescribes the displacement rather than the load for systems subjected to a single, concentrated force. This experience motivated a desire to employ prescribed load increments in the prebuckling range, and then switch to prescribed displacement increments in the post-buckling range to safely surpass the limit point. At first blush, a generalization of this formulation appears to require the solution of an unsymmetrical system and is therefore not attractive. The method was successfully generalized by Haisler et al. (1977) by a formulation that allows a displacement increment to be prescribed and computes the corresponding load intensity parameter for that increment. The method is able to surpass the limit point while retaining a symmetrical, albeit modified, structural stiffness matrix. Thus, a general form of direct displacement control of load steps was provided in which the load increment is chosen to constrain the displacement increment to a prescribed amount.

Batoz and Dhatt (1979) extended the above displacement control method to a fully incremental/iterative technique, common to nonlinear solution strategies, in which iteration to equilibrium occurs at constant displacement within each load step. Further, this method does not require the computational burden of modifying the stiffness matrix and is therefore more efficient.

The displacement control method has been generalized further by Powell and Simons (1981) and by Simons and Powell (1982). In this formulation the analyst is allowed more flexibility. The prescribed displacement increment is formulated as a linear combination of two displacement subincrements: one due to any unbalanced load from equilibrium iteration in the previous load step (which is a function of prescribed convergence tolerance), and the other due to a prescribed increment of external load. The method is shown to easily reduce to the previous methods by appropriate choices of the two coefficients in the expression for the linear combination of displacement increments.

Another method of automatic load step control within the context of a Newton-type linearization was provided by Riks (1972). In this paper, it is first demonstrated that equilibrium states do not exist in the neighborhood of limit points at values of loads in excess of the critical value, and so standard incremental/iterative solution methods are shown to fail at limit points. To surpass the limit point, Riks developed a method whereby equilibrium iteration occurs in load-displacement space, and the intersection of the load-displacement path with a set of planes perpendicular to the path is sought so that the incremental arc lengths of the path between intersections are constant. The planes are geometrical representations of constraint equations that require each arc length to be constant. The method has become known as an arc-length method for automatic load step control. There exist different forms of the constraint equation that, in turn, define different arc-length methods. Riks' algorithm is perhaps the most well-known arc-length method, having been implemented early into at least one widely used general purpose nonlinear finite element program.

The arc-length method employed in the analysis of the South Pole Dome is described by Bathe and Dvorkin (1983). They found the automatic load step control algorithm effective when two constraints are used depending on the response and load level. These two constraints are the spherical constant arc length method developed by Ramm (1981) and Crisfield (1981), which they use at points on the path far from critical points, and a constant increment of external work which they use near the critical points.

Further information on (tangent) constant arc-length methods may be found in papers by Rheinboldt and Riks (1983) and by Riks (1984). The associated mathematics of parameterized nonlinear systems, critical points such as limit points and single and multiple bifurcation points, etc., are advanced, but Riks' algorithm is said to be easily implemented into existing nonlinear finite element software frameworks. The method is not entirely satisfactory and more research and development is necessary to improve upon the robustness of all automatic load step control methods in the context of Newton-type linearizations.

Further research should acknowledge that real structures are likely to follow non-idealized or imperfection load-deflection paths. As a consequence, their instability will be associated with critical points that are regular limit points as contrasted with abrupt, bifurcation points. That is, additional dimensions representing imperfection parameters must be appended to the load-deflection space in the mathematical formulation of the problem. Ultimately, this would allow the engineer/analyst more control and flexibility while interacting with the software to determine the complete prebuckling and post-buckling response of real structures.

DISTRIBUTION LIST

AF 323 CES/DEEE (Tjoa), Mather AFB, CA; 6550 ABG/DER, Patrick AFB, FL; 6550 CES/DEEE, Patrick AFB, FL; 92d CES/DCME, Fairchild AFB, WA; AFIT/DET (Hudson), Wright-Patterson AFB, OH; AFIT/DET, Wright-Patterson AFB, OH; HQ ESD/DEE, Hanscom AFB, MA; HQ ESD/OCMS, Hanscom AFB, MA

AF HQ LETT (Cargo), Washington, DC

AFB 82nd ABG/DEMC, Williams, AZ; HQ MAC/DEEE, Scott AFB, IL; HQ SAC/IGSU (Holland), Offutt AFB, NE

AFESC RDC (Hayes), Tyndall AFB, FL; TST (Library), Tyndall AFB, FL

AFOSR NA, Bolling AFB, DC

AFSC DEEQ (P. Montoya), Peterson AFB, CO

NATL ACADEMY OF ENGRG Alexandria, VA

ARMY 416th ENCOM, Akron Survey Tm, Akron, OH; 501st Spt Gp, Ch Bldgs & Grnds Div, Yongsan, Korea; CSLA, Tech Ref Div, Huachuca, AZ; Ch of Engrs, DAEN-MPU, Washington, DC; ERADCOM Tech Supp Dir (DELSD-L), Ft Monmouth, NJ; FESA-EM (Krajewski), Ft Belvoir, VA; HQDA (DAEN-ZCM), Washington, DC; POJED-O, Okinawa, Japan; R&D Cmd, STRNC-US (J Sicgel), Natick, MA; SDC, CSSD-H-TF (McClellan), Huntsville, AL

ARMY ARADCOM STINFO Div, Dover, NJ

ARMY BELVOIR R&D CEN STRBE-AALO, Ft Belvoir, VA; STRBE-BLORE, Ft Belvoir, VA; STRBE-FS, Ft Belvoir, VA

ARMY CERL CERL-ZN, Champaign, IL; Library, Champaign, IL

ARMY CORPS OF ENGRS CENPS-ED-SD, Seattle, WA; HQ, DAEN-ECE-D (Paavola), Washington, DC; Library, Seattle, WA

ARMY DEPOT Letterkenny, SDSLE-SF, Chambersburg, PA

ARMY EHA HSHB-EW, Aberdeen Proving Grnd, MD

ARMY ENGR DIST LMVCO-A/Bentley, Vicksburg, MS; Phila, Lib, Philadelphia, PA

ARMY ENGR DIV ED-SY (Loyd), Huntsville, AL; HNDED-SY, Huntsville, AL

ARMY EWES Library, Vicksburg MS; WES-SS (Kiger), Vicksburg, MS; WESCV-Z (Whalin), Vicksburg, MS; WESGP-E, Vicksburg, MS; WESIM-C (N. Radhadrishnan), Vicksburg, MS

ARMY LMC Fort Lee, VA

ARMY LOGC ALC/ATCl-MS (Morrissett), Fort Lee, VA

ARMY MISSILE R&D CMD Ch, Docs, Sci Info Ctr, Arsenal, AL

ARMY MMRC DRXMR-SM (Lenoe), Watertown, MA

ARMY TRANS SCH ASTP-CDM, Fort Eustis, VA

ADMINSUPU PWO, Bahrain

BUREAU OF RECLAMATION D-1512 (GS DePuy), Denver, CO

CBC Code 10, Davisville, RI; Code 15, Port Hueneme, CA; Code 155, Port Hueneme, CA; Code 156F, Port Hueneme, CA; Code 430, Gulfport, MS; Library, Davisville, RI; PWO (Code 400), Gulfport, MS; PWO (Code 80), Port Hueneme, CA; Tech Library, Gulfport, MS

CBU 401, OIC, Great Lakes, IL

CINCLANTFLT CE Supp Plans Offr, Norfolk, VA

CINCPACFLT Code 41, Pearl Harbor, HI

COGARD R&DC Library, Groton, CT

COMCBLANT Code S3T, Norfolk, VA

COMCBPAC Diego Garcia Proj Offr, Pearl Harbor, HI

COMDT COGARD Library, Washington, DC

COMFAIR Med, Sec Offr, Naples, Italy

COMFLEACT PWO, Kadena, Japan; PWO, Sasebo, Japan

COMNAVAIRSYSCOM Code 41712, Washington, DC

COMNAVBEACHGRU ONE, CO, San Diego, CA

COMNAVFOR Korea, ENJ-P&O

COMNAVMARIANAS Code N4, Guam

COMNAVMEDCOM Sec Offr, Washington, DC

COMNAVRESFOR Code 08, New Orleans, LA

COMNAVSUPPFORANTARCTICA Code 50 (LDCR Barfield); DET, PWO, Christchurch, NZ

COMNAVSURF Code N42A, Norfolk, VA

COMOCEANSYS Lant, Code N9, Norfolk, VA

COMTRA Lant, SCE, Norfolk, VA

COMUSNAV CENT, Sec Offr, Pearl Harbor, HI

DFSC OWE, Alexandria, VA

DIA DB-6E1, Washington, DC; DB-6E2, Washington, DC; VP-TPO, Washington, DC

DIRSSP Tech Lib, Washington, DC

DOD DFSC-FE, Cameron Station, Alexandria, VA; Explos Safety Brd (Lib), Washington, DC

DOE Wind/Ocean Tech Div, Tobacco, MD

DTIC Alexandria, VA

DTNSRDC DET, Code 1250, Annapolis, MD; DET, Code 4120, Annapolis, MD
DTRCEN Code 172, Bethesda, MD; Code 1720, Bethesda, MD; Code 4111, Bethesda, MD
FAA Code APM-740 (Tomita), Washington, DC
FMFLANT CEC Offr, Norfolk, VA
FMFPAC SCIAD (G5), Camp HM Smith, HI
GIDEP OIC, Corona, CA
GSA Ch Engrg Br, PQB, Washington, DC
INTL MARITIME, INC D Walsh, San Pedro, CA
IRE-ITTD Input Proc Dir (R. Danford), Eagan, MN
KWAJALEIN MISRAN BMDSC-RKL-C
LIBRARY OF CONGRESS Sci & Tech Div, Washington, DC
MARCORBASE Code 4.01, Camp Pendleton, CA; Code 406, Camp Lejeune, NC; PWO, Camp Lejeune, NC; PWO, Camp Pendleton, CA; Pac, ACOS FE, Camp Butler, JA; Pac, FE, Camp Butler, JA
MARCORDIST 12, Code 4, San Francisco, CA
MARCORPS FIRST FSSG, Engr Supp Offr, Camp Pendleton, CA
MARITIME ADMIN MAR-770 (Corkrey), Washington, DC
MCLB Code 555, Albany, GA
MCAF Code CI44, Quantico, VA
MCAS PWO, Yuma, AZ
MCLB Code B520, Barstow, CA; PWC (Saehan), Barstow, CA
MCRD SCE, San Diego, CA
MCRDAC M & L Div Quantico, VA; NSAP Rep, Quantico, VA; PWO, Quantico, VA
NAF AROICC, Midway Island; Dir, Engrg Div, PWD, Atsugi, Japan; PWO, Atsugi, Japan
NAS Chase Fld, Code 18300, Beeville, TX; Chase Fld, PWO, Beeville, TX; Code 072E, Willow Grove, PA; Code 110, Adak, AK; Code 15, Alameda, CA; Code 163, Keflavik, Iceland; Code 1833, Corpus Christi, TX; Code 187, Jacksonville, FL; Code 70, South Weymouth, MA; Code 8, Patuxent River, MD; Code 83, Patuxent River, MD; Lead CPO, PWD, Self Help Div, Beeville, TX; Miramar, PWO, San Diego, CA; NI, Code 183, San Diego, CA; OL, Alameda, CA; PW Engrg (Branson), Patuxent River, MD; PWC-114 (PWO), Cubi Point, RP; PWD Maint Div, New Orleans, LA; PWO (Code 182) Bermuda; PWO, Cecil Field, FL; PWO, Dallas, TX; PWO, Glenview, IL; PWO, Keflavik, Iceland; PWO, Key West, FL; PWO, Kingsville TX; PWO, New Orleans, LA; PWO, Sigonella, Italy; PWO, South Weymouth, MA; PWO, Willow Grove, PA; SCE, Barbers Point, HI; SCE, Norfolk, VA; Whidbey Is, PW-2, Oak Harbor, WA; Whiting Fld, PWO, Milton, FL
NATL BUREAU OF STANDARDS R Chung, Gaithersburg, MD
NAVAIRDEVCEN Code 832, Warminster, PA; Code 8323, Warminster, PA
NAVAIRENGCEN Code 182, Lakehurst, NJ; PWO, Lakehurst, NJ
NAVAIRTESTCEN PWO, Patuxent River, MD
NAVAUDSVCHQ Director, Falls Church VA
NAVAVNDEPOT Code 61000, Cherry Point, NC; Code 640, Pensacola, FL
NAVCAMS PWO, Norfolk, VA; SCE (Code N-7), Naples, Italy
NAVCHAPGRU Code 30, Williamsburg, VA; Code 60, Williamsburg, VA
NAVCOASTSYSCEN CO, Panama City, FL; Code 2360, Panama City, FL; Code 630, Panama City, FL; Tech Library, Panama City, FL
NAVCOMMSTA Code 401, Nea Makri, Greece
NAVCONSTRACEN Code 00U15, Port Hueneme, CA; Code B-1, Port Hueneme, CA; Code T12, Gulfport, MS
NAVEDTRAPRODEVCEN Tech Lib, Pensacola, FL
NAVELEXCEN DET, OIC, Winter Harbor, ME
NAVEODTECHCEN Tech Library, Indian Head, MD
NAVFAC Centerville Bch, PWO, Ferndale, CA; PWO (Code 50), Brawdy Wales, UK; PWO, Oak Harbor, WA
NAVFACENGCOM 04B4 *Cecilio), Alexandria, VA; Code 00, Alexandria, VA; Code 03, Alexandria, VA; Code 032F, Alexandria, VA; Code 03T (Essoglou), Alexandria, VA; Code 04A, Alexandria, VA; Code 04A1, Alexandria, VA; Code 04A1D, Alexandria, VA; Code 04A3, Alexandria, VA; Code 04BE (Wu), Alexandria, VA; Code 06, Alexandria, VA; Code 0631 (Cyphers), Alexandria, VA; Code 07M (Gross), Alexandria, VA; Code 09M124 (Lib), Alexandria, VA
NAVFACENGCOM - CHES DIV, FPO-1PL, Washington, DC
NAVFACENGCOM - LANT DIV, Br Ofc, Dir, Naples, Italy; Code 1112, Norfolk, VA; Code 405, Norfolk, VA; Library, Norfolk, VA
NAVFACENGCOM - NORTH DIV, Code 04, Philadelphia, PA; Code 04AL, Philadelphia, PA; Code 11, Philadelphia, PA; Code 202.2, Philadelphia, PA
NAVFACENGCOM - PAC DIV, Code 09P, Pearl Harbor, HI; Code 101 (Kyi), Pearl Harbor, HI; Code 2011, Pearl Harbor, HI; Code 402, Pearl Harbor, HI; Library, Pearl Harbor, HI
NAVFACENGCOM - SOUTH DIV, Code 04A3, Charleston, SC; Code 1112, Charleston, SC; Code 406, Charleston, SC; Library, Charleston, SC

NAVFACENGCOM - WEST DIV, 09P/20, San Bruno, CA; Code 04A2.2 (Lib), San Bruno, CA; Code 04B, San Bruno, CA; Code 09B, San Bruno, CA; Code 101.1, San Diego, CA; Pac NW Br Offc, Code C/50, Silverdale, WA

NAVFACENGCOM CONTRACTS Code 460, Portsmouth, VA; DROICC, Lemoore, CA; Earle, ROICC, Colts Neck, NJ; North Bay, Code 1042.AA, Vallejo, CA; OICC, Guam; OICC/ROICC, Norfolk, VA; ROICC (Code 913), Everett, WA; ROICC, Corpus Christi, TX; ROICC, Crane, IN; ROICC, Keflavik, Iceland; ROICC, Point Mugu, CA; ROICC, Quantico, VA; ROICC, Twentynine Palms, CA; ROICC, Virginia Beach, VA; SW Pac, OICC, Manila, RP; Trident, OICC, St Marys, GA

NAVFUEL DET OIC, Yokohama, Japan

NAVHOSP CO, Millington, TN; SCE (Knapowski), Great Lakes, IL; SCE, Camp Pendleton, CA; SCE, Pensacola, FL

NAVMAG SCE, Subic Bay, RP

NAVMARCORESCEN LTJG Davis, Raleigh, NC

NAVMEDCOM SE REG, Hd, Fac Mgmt Dept, Jacksonville, FL; SWREG, Head, Fac Mgmt Dept, San Diego, CA; SWREG, OICC, San Diego, CA

NAVOCEANCOMCEN CO, Guam, Mariana Islands; Code EES, Guam, Mariana Islands

NAVOCEANO Code 6200 (M Paige), Bay St. Louis, MS

NAVOCEANSYSCEN Code 9642B, San Diego, CA

NAVPGSCOL PWO, Monterey, CA

NAVPHIBASE PWO, Norfolk, VA; SCE, San Diego, CA

NAVSCOLCECOFF Code C35, Port Hueneme, CA; Code C44A, Port Hueneme, CA

NAVSCSCOL PWO, Athens, GA

NAVSEACENPAC Code 32, San Diego, CA

NAVSEASYSCOM Code 05M, Washington, DC; Code 05R12, Washington, DC; Code PMS296L22 (J Rekas), Washington, DC

NAVSECGRU Code G43, Washington, DC

NAVSECGRUACT PWO (Code 40), Edzell, Scotland

NAVSHIPREPFAC Library, Guam; SCE, Subic Bay, RP; SCE, Yokosuka, Japan

NAVSHIPYD Code 202.4, Long Beach, CA; Code 202.5 (Library), Bremerton, WA; Code 308.3, Pearl Harbor, HI; Code 440, Portsmouth, NH; Code 443, Bremerton, WA; Library, Portsmouth, NH; Mare Island, Code 202.13, Vallejo, CA; Mare Island, Code 280, Vallejo, CA; Mare Island, Code 404, Vallejo, CA; Mare Island, Code 421, Vallejo, CA; Mare Island, PWO, Vallejo, CA; Norfolk, Code 380, Portsmouth, VA; Norfolk, Code 411, Portsmouth, VA; Norfolk, Code 440, Portsmouth, VA; Norfolk, Code 442.2, Portsmouth, VA; PWO, Bremerton, WA; PWO, Charleston, SC

NAVSTA CO, Long Beach, CA; CO, Roosevelt Roads, PR; Code 423, FPBO Guantanamo Bay; Code N4215, Mayport, FL; Engr Div, PWD, Rodman, Panama Canal; Engrg Dir, Rota, Spain; PWO, Mayport, FL; SCE, Guam, Marianas Islands; SCE, San Diego, CA; SCE, Subic Bay, RP; WC 93, Guantanamo Bay, Cuba

NAVSUPPACT PWO, Naples, Italy

NAVSWC Code E211 (Miller), Dahlgren, VA; Code G-34, Dahlgren, VA; Code W42 (R Ponzetto), Dahlgren, VA; DET, White Oak Lab, Code H-101, Silver Spring, MD; DET, White Oak Lab, Code WSO, Silver Spring, MD; PWO, Dahlgren, VA

NAVWARCOL Code 24, Newport, RI

NAVWPNCEN AROICC, China Lake, CA; Code 2637, China Lake, CA; PWO (Code 266), China Lake, CA

NAVWPNSTA Dir, Maint Control, PWD, Concord, CA; Earle, Code 0922, Colts Neck, NJ; Earle, PWO (Code 09B), Colts Neck, NJ; Engrg Div, PWD, Yorktown, VA; PWO, Charleston, SC; PWO, Seal Beach, CA; PWO, Yorktown, VA

NAVWPNSUPPCEN PWO, Crane, IN

NETC Code 42, Newport, RI; PWO, Newport, RI

NCR 20, CO; 20, Code R70

NEESA Code 111E (McClaine), Port Hueneme, CA; Code 113M, Port Hueneme, CA

NMCB 3, Ops Offr; 40, CO; 5, Ops Dept; 62, Engrg Offr; 74, CO

NOAA Joseph Vadus, Rockville, MD

NRL Code 2511, Washington, DC; Code 5800, Washington, DC

NSC Cheatham Annex, PWO, Williamsburg, VA; Code 54.1, Norfolk, VA; SCE, Norfolk, VA

NSD SCE, Subic Bay, RP

NSF POLAR G. Fitzsimmons, Washington, DC; R. Hachle, Washington, DC

NUSC DET Code 3232 (Varley), New London, CT; Code 44 (RS Munn), New London, CT; Code TA131, New London, CT; Lib (Code 4533), Newport, RI

OCNR Code 1121 (EA Silva), Arlington, VA; Code 33, Arlington, VA; Code 432 (Kushner), Arlington, VA

OFFICE OF SECRETARY OF DEFENSE OASD (A&L), L(EP), Washington, DC

PACMISRANFAC HI Area, PWO, Kekaha, HI

PHIBCB 1, CO, San Diego, CA; 1, P&E, San Diego, CA; 2, CO, Norfolk, VA

PMTC Code 1018, Point Mugu, CA; Code 5041, Point Mugu, CA

PWC ACE Offiee, Norfolk, VA; Code 10, Great Lakes, IL; Code 10, Oakland, CA; Code 101 (Library), Oakland, CA; Code 1011, Pearl Harbor, HI; Code 102, Oakland, CA; Code 123-C, San Diego, CA; Code 30, Norfolk, VA; Code 400, Great Lakes, IL; Code 400, Oakland, CA; Code 400, Pearl Harbor, HI; Code

400, San Diego, CA; Code 420, Great Lakes, IL; Code 420, Oakland, CA; Code 420B (Waid), Subic Bay, RP; Code 421 (Quin), San Diego, CA; Code 421 (Reynolds), San Diego, CA; Code 422, San Diego, CA; Code 423, San Diego, CA; Code 424, Norfolk, VA; Code 425 (Kaya), Pearl Harhor, HI; Code 500, Great Lakes, IL; Code 500, Oakland, CA; Code 600, Great Lakes, IL; Code 612, Pearl Harbor, HI; Code 613, San Diego, CA; Library (Code 134), Pearl Harbor, HI; Library, Guam, Mariana Islands; Library, Norfolk, VA; Library, Pensacola, FL; Library, Yokosuka, Japan; Tech Library, Subic Bay, RP

SAN DIEGO PORT Port Fac, Proj Engr, San Diego, CA

SPCC PWO (Code 08X), Mechanicsburg, PA

SUBASE Bangor, PWO (Code 8323), Bremerton, WA

SUPSHIP Tech Library, Newport News, VA

HAYNES & ASSOC H. Haynes, P.E., Oakland, CA

US DEPT OF INTERIOR Natl Park Svc, RMR/PC, Denver, CO

USCINCPAC Code J44, Camp HM Smith, HI

USDA Ext Serv (T Maher), Washington, DC; For Svc Reg 8, (Bowers), Atlanta, GA; For Svc, Reg Bridge Engr, Aloha, OR; For Svc, Tech Engrs, Washington, DC

USNA Ch, Mech Engrg Dept, Annapolis, MD; Ocean Engrg Dept (McCormick), Annapolis, MD; PWO, Annapolis, MD; Sys Engrg, Annapolis, MD

ADVANCED TECHNOLOGY, INC Ops Cen Mgr (Bednar), Camarillo, CA

CALIFORNIA STATE UNIVERSITY C.V. Chelapati, Long Beach, CA

CITY OF BERKELEY PW, Engr Div (Harrison), Berkeley, CA

CITY OF LIVERMORE Dackins, PE, Livermore, CA

CLARKSON COLL OF TECH CE Dept (Batson), Potsdam, NY

COLORADO STATE UNIVERSITY CE Dept (Vanderbilt), Ft Collins, CO

CORNELL UNIVERSITY Civil & Environ Engrg (Dr. Kulhawy), Ithaca, NY; Library, Ithaca, NY

DAMES & MOORE Library, Los Angeles, CA

FLORIDA ATLANTIC UNIVERSITY Ocean Engrg Dept (Su), Boca Raton, FL

FLORIDA INST OF TECH CE Dept (Kalajian), Melbourne, FL

GEORGIA INSTITUTE OF TECHNOLOGY CE Scol (Kahn), Atlanta, GA

INSTITUTE OF MARINE SCIENCES Library, Port Aransas, TX

JOHNS HOPKINS UNIV CE Dcpt (Jones), Baltimore, MD

LAWRENCE LIVERMORE NATL LAB FJ Tokarz, Livermore, CA; L-654, Plant Engrg Lib, Livermore, CA

LEHIGH UNIVERSITY Linderman Library, Bethlehem, PA

MICHIGAN TECH UNIVERSITY CE Dcpt (Haas), Houghton, MI

MIT Engrg Lib, Cambridge, MA; Lib, Tech Reports, Cambridge, MA; RV Whitman, Cambridge, MA

NATL ACADEMY OF SCIENCES NRC, Naval Studies Bd, Washington, DC

NEW MEXICO SOLAR ENERGY INST Dr. Zwibel, Las Cruces, NM

NEW YORK-NEW JERSEY PORT AUTH R&D Engr (Yontar), Jersey City, NJ

NORTHWESTERN UNIV CE Dept (Belytschko), Evanston, IL

OREGON STATE UNIVERSITY CE Dept (Hicks), Corvallis, OR; CE Dept (Leonard), Corvallis, OR

PENNSYLVANIA STATE UNIVERSITY Gotolski, University Park, PA; Rsch Lab (Snyder), State College, PA

PORTLAND STATE UNIVERSITY Engrg Dept (Migliori), Portland, OR

PURDUE UNIVERSITY CE Scol (Leonards), W. Lafayette, IN; Engrg Lib, W. Lafayette, IN

SAN DIEGO STATE UNIV CE Dept (Krishnamoorthy), San Diego, CA

SEATTLE UNIVERSITY CE Dcpt (Schwaegler), Seattle, WA

SOUTHWEST RSCH INST Energetic Sys Dept (Esparza), San Antonio, TX; J. Hokanson, San Antonio, TX; King, San Antonio, TX; R. DeHart, San Antonio TX

STANFORD UNIVERSITY App Mech Div (Hughes), Stanford, CA

STATE UNIVERSITY OF NEW YORK CE Dcpt (Reinhorn), Buffalo, NY; CE Dcpt, Buffalo, NY

TECH UTILIZATION K Willinger, Washington, DC

TEXAS A&I UNIVERSITY Civil & Mech Engr Dept, Kingsville, TX

TEXAS A&M UNIVERSITY CE Dept (Niedzwecki), College Station, TX; Ocean Engr Proj, College Station, TX

UNIVERSITY OF CALIFORNIA CE Dept (Fenves), Berkeley, CA; CE Dept (Gerwick), Berkeley, CA; CE Dept (Herrmann), Davis, CA; CE Dept (Kutter), Davis, CA; CE Dept (Romstad), Davis, CA; CE Dept (Shen), Davis, CA; CE Dept (Taylor), Berkeley, CA; CE Dept (Taylor), Davis, CA; Engrg (Williamson), Berkeley, CA; Geotech Model Cen (Cheney), Davis, CA; Mech Engrg Dept (Bayo), Santa Barbara, CA; Naval Arch Dept, Berkeley, CA

UNIVERSITY OF COLORADO CE Dept (Hon-Yim Ko), Boulder, CO

UNIVERSITY OF HAWAII CE Dept (Chiu), Honolulu, HI; Manoa, Library, Honolulu, HI; Ocean Engrg Dept (Ertekin), Honolulu, HI

UNIVERSITY OF ILLINOIS Arch Scol (Kim), Champaign, IL; CE Dept (W. Gamble), Urbana, IL; CE Lab (Abrams), Urbana, IL; CE Lab (Pecknold), Urbana, IL; Library, Urbana, IL; M.T. Davisson, Urbana, IL; Metz Ref Rm, Urbana, IL

UNIVERSITY OF MICHIGAN CE Dept (Richart), Ann Arbor, MI

UNIVERSITY OF NEBRASKA Polar Ice Coring Office, Lincoln, NE

UNIVERSITY OF NEW MEXICO JM Carson, Albuquerque, NM; NMERI (Falk), Albuquerque, NM; NMERI (Leigh), Albuquerque, NM
UNIVERSITY OF PENNSYLVANIA Dept of Arch (P. McCleary), Philadelphia, PA
UNIVERSITY OF TEXAS CE Dept (Thompson), Austin, TX; ECJ 4.8 (Breen), Austin, TX; ECJ 5.402 (Friedrich), Austin, TX
UNIVERSITY OF WASHINGTON CE Dept (Mattock), Seattle, WA
UNIVERSITY OF WISCONSIN Great Lakes Studies Cen, Milwaukee, WI
WASHINGTON DHHS, OFE/PHS (Ishihara), Seattle, WA
ADINA ENGRG, INC Walczak, Watertown, MA
AMERICAN CONCRETE INSTITUTE Library, Detroit, MI
AMETEK OFFSHORE RSCH Santa Barbara, CA
APPLIED RSCH ASSOC, INC Higgins, Albuquerque, NM
APPLIED SCI ASSOC, INC White, Orlando, FL
APPLIED SYSTEMS R. Smith, Agana, Guam
ARMSTRONG AERO MED RSCH LAB Ovenshire, Wright-Patterson AFB, OH
ARVID GRANT & ASSOC Olympia, WA
ATLANTIC RICHFIELD CO RE Smith, Dallas, TX
AWWA RSCH FOUNDATION R. Heaton, Denver, CO
BATTELLE D Frink, Columbus, OH
BECHTEL NATL, INC Woolston, San Francisco, CA
BETHLEHEM STEEL CO Engrg Dept (Dismuke), Bethlehem, PA
BRITISH EMBASSY Sci & Tech Dept (Wilkins), Washington, DC
BROWN & ROOT Ward, Houston, TX
CANADA Viateur De Champlain, D.S.A., Matane, Canada
CHAS T MAIN, INC RC Goyette, Portland, OR
CHEVRON OIL FLD RSCH CO Strickland, La Habra, CA
CLARENCE R JONES, CONSULTN, LTD Augusta, GA
COLLINS ENGRG, INC M Garlich, Chicago, IL
CONRAD ASSOC Luisoni, Van Nuys, CA
CONSOER TOWNSEND & ASSOC Schramm, Chicago, IL
CONSTRUCTION TECH LABS, INC Dr. Corley, Skokie, IL
DILLINGHAM CONSTR CORP (HD&C), F McHale, Honolulu, HI
DRAVO CORP Wright, Pittsburg, PA
DURLACH, O'NEAL, JENKINS & ASSOC Columbia, SC
ENERCOMP H. Amistadi, Brunswick, ME
EVALUATION ASSOC, INC MA Fedele, King of Prussia, PA
FUGRO INTER-GULF CO Library, Houston, TX
GRUMMAN AEROSPACE CORP Tech Info Ctr, Bethpage, NY
HJ DEGENKOLB ASSOC W Murdough, San Francisco, CA
HUGHES AIRCRAFT CO Tech Doc Cen, El Segundo, CA
IFFLAND KAVANAGH WATERBURY, PC New York, NY
JOHN J MC MULLEN ASSOC Library, New York, NY
LAYTON & SELL, INC, P.S. Mfg Rsch Dept (Edwards), Marietta, GA
LEO A DALY CO Honolulu, HI
LIN OFFSHORE ENGRG P. Chow, San Francisco CA
LINDA HALL LIBRARY Doc Dept, Kansas City, MO
LOCKHEED Rsch Lab (Nour-Omid), Palo Alto, CA
MARATHON OIL CO Gamble, Houston, TX
MARC ANALYSIS RSCH CORP Hsu, Palo Alto, CA
MARITECH ENGRG Donoghue, Austin, TX
MOBIL R & D CORP Offshore Engrg Lib, Dallas, TX
EDWARD K NODA & ASSOC Honolulu, HI
NEW ZEALAND NZ Concrete Rsch Assoc, Library, Porirua
PACIFIC MARINE TECH (M. Wagner) Duvall, WA
PMB SYS ENGRG, INC Bea, San Francisco, CA
PRESNELL ASSOC, INC DG Presnell, Jr, Louisville, KY
SANDIA LABS Library, Livermore, CA
SARGENT & HERKES, INC JP Pierce, Jr, New Orleans, LA
SAUDI ARABIA King Saud Univ, Rsch Cen, Riyadh
SEATECH CORP Peroni, Miami, FL
SHELL OIL CO E Doyle, Houston, TX; E&P Civil Engrg, Houston, TX
SIMPSON, GUMPERTZ & HEGER, INC E Hill, CE, Arlington, MA
SRI INTL Engrg Mech Dept (Simons), Menlo Park, CA
TANDEMLOC, INC J DiMartino, Jr, Ronkonkoma, NY

TRW INC Crawford, Redondo Beach, CA; Dai, San Bernardino, CA; Engr Library, Cleveland, OH; M Katona, San Bernardino, CA
WEIDLINGER ASSOC F.S. Wong, Palo Alto, CA
WELLSPRING COMM H Zarecor, Marshall, VA
WESTINGHOUSE ELECTRIC CORP Library, Pittsburg, PA
WISS, JANNEY, ELSTNER, & ASSOC DW Pfeifer, Northbrook, IL
WOODWARD-CLYDE CONSULTANTS R Dominguez, Houston, TX; W Reg, Lib, Walnut Creek, CA
BESIER, RF CE, Old Saybrook, CT
BROWN, ROBERT University, AL
BULLOCK, TE La Canada, CA
CHAO, JC Houston, TX
CLARK, T. Redding, CA
COX, J Davis, CA
HAYNES, B. Austin, TX
HEUZE, F Alamo, CA
HIRSCH & CO L Hirsch, San Diego, CA
MEDWADOWSKI, SJ Consult Struct Engr, San Francisco, CA
NIEDORODA, AW Houston, TX
PADILLA, LM Oxnard, CA
PETERSEN, CAPT N.W. Pleasanton, CA
QUIRK, J Panama City, FL
SPIELVOGEL, L Wyncote, PA
STEVENS, TW Long Beach, MS
ULASZEWSKI, CDR T.J. Honolulu, HI
VAN ALLEN, B Kingston, NY
WEBSTER, R Brigham City, UT

INSTRUCTIONS

The Naval Civil Engineering Laboratory has revised its primary distribution lists. The bottom of the label on the reverse side has several numbers listed. These numbers correspond to numbers assigned to the list of Subject Categories. Numbers on the label corresponding to those on the list indicate the subject category and type of documents you are presently receiving. If you are satisfied, throw this card away (or file it for later reference).

If you want to change what you are presently receiving:

- Delete – mark off number on bottom of label.
- Add – circle number on list.
- Remove my name from all your lists – check box on list.
- Change my address – line out incorrect line and write in correction **(PLEASE ATTACH LABEL).**
- Number of copies should be entered after the title of the subject categories you select.

Fold on line below and drop in the mail.

Note: Numbers on label but not listed on questionnaire are for NCEL use only, please ignore them.

Fold on line and staple.

DEPARTMENT OF THE NAVY

NAVAL CIVIL ENGINEERING LABORATORY
PORT HUENEME, CALIFORNIA 93043-5003

OFFICIAL BUSINESS
PENALTY FOR PRIVATE USE, $300
NCEL-2700/4 (REV. 10-87)
0930-LL-L70-0044

BUSINESS REPLY CARD

FIRST CLASS PERMIT NO. 69

POSTAGE WILL BE PAID BY ADDRESSEE

Commanding Officer
Code L08B
Naval Civil Engineering Laboratory
Port Hueneme, California 93043-5003

NO POSTAGE
NECESSARY
IF MAILED
IN THE
UNITED STATES

DISTRIBUTION QUESTIONNAIRE

The Naval Civil Engineering Laboratory is revising its primary distribution lists.

SUBJECT CATEGORIES

1 **SHORE FACILITIES**
2 Construction methods and materials (including corrosion control, coatings)
3 Waterfront structures (maintenance/deterioration control)
4 Utilities (including power conditioning)
5 Explosives safety
6 Aviation Engineering Test Facilities
7 Fire prevention and control
8 Antenna technology
9 Structural analysis and design (including numerical and computer techniques)
10 Protective construction (including hardened shelters, shock and vibration studies)
11 Soil/rock mechanics
14 Airfields and pavements

15 **ADVANCED BASE AND AMPHIBIOUS FACILITIES**
16 Base facilities (including shelters, power generation, water supplies)
17 Expedient roads/airfields/bridges
18 Amphibious operations (including breakwaters, wave forces)
19 Over-the-Beach operations (including containerization, materiel transfer, lighterage and cranes)
20 POL storage, transfer and distribution

28 **ENERGY/POWER GENERATION**
29 Thermal conservation (thermal engineering of buildings, HVAC systems, energy loss measurement, power generation)
30 Controls and electrical conservation (electrical systems, energy monitoring and control systems)
31 Fuel flexibility (liquid fuels, coal utilization, energy from solid waste)
32 Alternate energy source (geothermal power, photovoltaic power systems, solar systems, wind systems, energy storage systems)
33 Site data and systems integration (energy resource data, energy consumption data, integrating energy systems)
34 **ENVIRONMENTAL PROTECTION**
35 Solid waste management
36 Hazardous/toxic materials management
37 Wastewater management and sanitary engineering
38 Oil pollution removal and recovery
39 Air pollution
44 **OCEAN ENGINEERING**
45 Seafloor soils and foundations
46 Seafloor construction systems and operations (including diver and manipulator tools)
47 Undersea structures and materials
48 Anchors and moorings
49 Undersea power systems, electromechanical cables, and connectors
50 Pressure vessel facilities
51 Physical environment (including site surveying)
52 Ocean-based concrete structures
54 Undersea cable dynamics

TYPES OF DOCUMENTS

85 Techdata Sheets
86 Technical Reports and Technical Notes
82 NCEL Guides & Abstracts
☐ None—remove my name
83 Table of Contents & Index to TDS
91 Physical Security

DEPARTMENT OF THE NAVY

NAVAL CIVIL ENGINEERING LABORATORY
PORT HUENEME, CALIFORNIA 93043

521 - 93.003 - 25

1

Library
DOD Explosives Safety Brd
Hoffman Bldg I, Rm 856C
2461 Eisenhower Ave
Alexandria, VA 22331-0600

5,9,10,78,86